

# Space and time correlations for diffusion models with prompt and delayed birth-and-death events

Théophile Bonnet,<sup>\*</sup> Davide Mancusi,<sup>†</sup> and Andrea Zoia<sup>‡</sup>

*Université Paris-Saclay, CEA, Service d'Etudes des Réacteurs et de Mathématiques Appliquées, 91191, Gif-sur-Yvette, France*

(Dated: March 4, 2022)

Understanding the statistical properties of a collection of individuals subject to random displacements and birth-and-death events is key to several applications in physics and life sciences, encompassing the diagnostic of nuclear reactors and the analysis of epidemic patterns. Previous investigations of the critical regime, where births and deaths balance on average, have shown that highly non-Poissonian fluctuations might occur in the population, leading to spontaneous spatial clustering, and eventually to a “critical catastrophe”, where fluctuations can result in the extinction of the population. A milder behaviour is observed when the population size is kept constant: the fluctuations asymptotically level off and the critical catastrophe is averted. In this paper, we shall extend these results by considering the broader class of models with prompt and delayed birth-and-death events, which mimic the presence of precursors in nuclear reactor physics or incubation in epidemics. We shall consider models with and without population control mechanisms. Analytical or semi-analytical results for the density, the two-point correlation function and the mean-squared pair distance will be derived and compared to Monte Carlo simulations, which will be used as a reference.

## I. INTRODUCTION

Many systems of interest in physics and life sciences can be modeled in terms of a collection of individuals undergoing random displacements coupled with birth-and-death events of the Galton-Watson type [1–6]. Two prominent examples concern for instance the spread of epidemics and the propagation of neutron-induced fission chains in nuclear reactors. For epidemics, the displacements are those of the infected, i.e., the carriers of the pathogen; births are due to the appearance of new infected individuals due to contacts of the infected with susceptibles; and deaths are due to the transitions of the infected to the recovered (or possibly back to the susceptibles) [2]. For neutrons, displacements result from free flights and from scattering collisions with the nuclei of the traversed media, leading to random re-orientations of the flight directions; births are due to fission events, which split the nuclei and emit extra neutrons; and deaths are due to collisions leading to sterile captures, whereupon the neutron life is terminated [3]. In some models, a fraction of the birth events may occur with a delay: for epidemics, delayed infections are related to the incubation time of the pathogen [7], whereas in reactor physics the appearance of delayed neutrons is due to the de-excitation of the fission fragments, which may emit extra neutrons after exponentially distributed decay times [3].

By virtue of their common ingredients, the mathematical descriptions of epidemics and fission chains strikingly share many features [1], although model-specific traits must be taken into account in realistic applications. The evolution of populations subject to diffusion, births and deaths can be described by a variety of frameworks, encompassing deterministic and stochastic approaches, each having distinct advantages and shortcomings [8, 9]. When births are compensated by deaths, the number of individuals is constant on average, and the system is said

to be critical [1]: this regime is usually realized in nuclear reactors, where physical parameters are precisely tuned so that the energy released by fission is stationary [3]. The critical regime also plays a central role in epidemics, non-trivially affecting control policies in the transition between the super-critical and the sub-critical phases [10]. If the number of individuals is large, as in later stages of epidemics or in nuclear reactor operated at full power, the average behaviour of the population is sufficient to completely characterize the system. On the contrary, if the number of individuals is small, which is the case e.g. for epidemics during the early outbreak phases and for nuclear reactors operated at low power, the fluctuations around the average might be relevant and a stochastic description is required [3, 5]. In this case, one either uses deterministic methods to solve the equations for the statistical moments of the population, or Monte Carlo methods to sample the random dynamics.

Although mean-field zero-dimensional approaches can provide a condensed representation of the system dynamics, stochastic models accounting for the full description of the spatial behavior of the population are of utmost importance, in that they are key e.g. to characterizing the extent of epidemic outbursts [11–13] or to detecting possible malfunctioning or power tilts in nuclear reactors [3, 6, 14]. Modern state-of-the-art Monte Carlo simulation codes allow addressing real-world applications with unprecedented accuracy and have been successfully used to compute the lower-order moments of the populations, namely, the average number of individuals  $\mathbb{E}[n_V](t)$  in a given spatial region  $V$  at time  $t$  and the two-point correlation function  $\mathbb{E}[n_{V_1} n_{V_2}](t_1, t_2)$  between two regions  $V_1$  and  $V_2$  at times  $t_1$  and  $t_2$  [14–17]. The analysis carried out with highly sophisticated simulation codes can be effectively complemented by the investigation of simplified mathematical models that avoid unnecessary complication and yet retain the key physical ingredients, possi-

bly leading to semi-quantitative predictions. In the context of reactor physics, explicit expressions for the average number of individuals and the two-point correlation function of the population have been recently derived, for one such model combining a Galton-Watson process with Brownian diffusion in bounded domains [18–20]. Inspection of the resulting solutions of the moment equations shows that, in the critical regime, the birth-and-death events will induce strongly non-Poissonian fluctuations in the number of individuals being present at each spatial site, which lead to a wild spatial patchiness (clustering) instead of the expected uniform density. Eventually, the population will face a “critical catastrophe”, where fluctuations can result in an extinction event. Furthermore, it has been shown that the interplay between prompt and delayed birth-and-death events affects the time scales of clustering and of the critical catastrophe [19, 20]. Although these investigations were mainly motivated by applications pertaining to nuclear reactor physics, the main findings would carry over to the spatial behaviour of epidemics, with minimal modifications. For instance, it is known that around criticality all realistic epidemiological models display large fluctuations that dominate the dynamical behaviour of the system, regardless of the specific details of the infection process [10].

In the basic formulation of these models, the size of the population is free to evolve according to the stochastic rules of the process, without any constraint. In practice, epidemics are subject to health policies and restrictions, and nuclear reactors are similarly endowed with intrinsic (physics-based) and external control mechanisms to prevent power drifts. A simple, yet effective way of mimicking some form of feedback acting against variations in the number of individuals consists in enforcing the population size to be exactly constant. Such control mechanisms have been shown to have a dramatic impact on the evolution of the fluctuations, compared to the free case. In constrained models, clustering is still present at the local scale, but the spatial fluctuations at the global scale asymptotically level off and the critical catastrophe is averted [20, 21]. For the sake of simplicity, so far such models with population control have only addressed prompt birth-and-death events. Within the framework of a simplified nuclear reactor model, in this paper we will extend these findings by introducing a generalized approach to the enforcement of population control, where the hypothesis of constant population size is relaxed and delayed birth events are explicitly considered. Analytical or semi-analytical formulas for the neutron spatial density, the two-point correlation function and the mean-squared pair distance between particles will be derived and compared to Monte Carlo simulations, which will be used as a reference.

This work is organised as follows: in Sec. II we present the stochastic model that will be used throughout this manuscript, detail the underlying hypotheses, and introduce relevant observables. In Sec. III we derive the key results for the evolution of individuals without popula-

tion control. In Sec. IV we derive the key results for a collection of individuals under different sorts of population control. Conclusions will be finally drawn in Sec. V. In order to improve readability, cumbersome calculations will be relegated to the Appendix.

## II. A SIMPLE STOCHASTIC MODEL FOR NUCLEAR REACTOR PHYSICS

To fix the ideas and the vocabulary, in the following we choose to work with a nuclear reactor model, but most of the results presented in this paper would apply also to epidemics.

In the simplest incarnation of our nuclear reactor model [19], we represent the random movement of neutrons as Brownian motion with a diffusion coefficient  $\mathcal{D}$ , and we use a Galton-Watson birth-death process to describe fission and absorption. Each neutron undergoes sterile capture at a rate  $\gamma$  and fission events at a rate  $\beta$ . Captured neutrons are simply killed. When fission occurs, a random number of new neutrons are emitted at the position of the incident neutron, which is killed [3]. Part of the fission neutrons are emitted instantaneously and are known as *prompt* neutrons: the probability to emit  $k$  prompt neutrons is denoted as  $p_k$ . *Delayed* neutrons may further appear at the spatial site of a fission event after a random, exponentially distributed time with rate  $\lambda$ , corresponding to the nuclear decay of certain excited fission fragments, known as *delayed neutron precursors* [3]. We denote by  $q_k$  the probability that  $k$  delayed neutron precursors are created at a fission event. For illustration, some representative neutron and precursor histories are shown in Fig. 1. In nuclear reactors, the average precursor decay time  $1/\lambda$  is typically much larger than the average neutron lifetime  $1/(\gamma + \beta)$ . Furthermore, denoting respectively by  $\nu_{p,1} = \sum_k k p_k$  and  $\nu_{d,1} = \sum_k k q_k$  the average number of prompt and delayed neutrons resulting from fission, we typically have  $\nu_{p,1} \gg \nu_{d,1}$  [3]. For reasons that will become clear in the following, we are using the notation  $\nu_{p,l}$  and  $\nu_{d,l}$  to indicate the  $l$ -th falling factorial moments of the number of neutrons and precursors produced from fission, respectively, with

$$\nu_{p,l} = \sum_{k=0}^{\infty} k(k-1)\dots(k-l+1)p_k \quad (1)$$

and

$$\nu_{d,l} = \sum_{k=0}^{\infty} k(k-1)\dots(k-l+1)q_k. \quad (2)$$

For the sake of simplicity, our model neglects the energy dependence of the neutron-matter interaction rates. Furthermore, the spatial structure of the reactor core will be simplified by assuming that all the material properties (diffusion coefficient, fission and capture rates) are

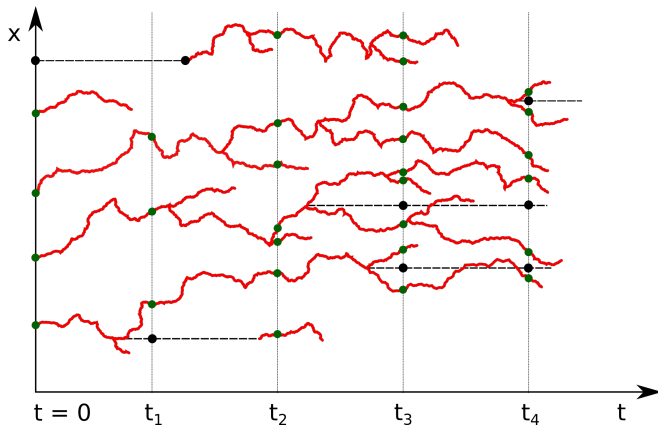


FIG. 1. Schematic illustration of the evolution of neutrons and precursors in the simplest model (anarchic model). At time  $t = 0$ , 4 neutrons and 1 precursor are present. Neutrons (red solid lines) diffuse and undergo fission and capture; precursors (dashed black lines) do not diffuse. When they decay, they are replaced by a neutron at the same position. Because of the birth-death process, the total number of neutrons and the total number of precursors fluctuate.

homogeneous. All the physical parameters are taken to be uniform in space and constant in time. Contrary to Ref. 19, which considered unbounded systems, here the reactor will be modeled as a finite-size box with reflection (Neumann) boundary conditions, mimicking the fact that in nuclear reactors neutron leakage from the core is deliberately kept small. To simplify matters even further, we will focus on one-dimensional systems, which are more easily amenable to analytical solutions: in what follows, we will thus consider a one-dimensional reactor of half-size  $L$ , i.e. the  $[-L, L]$  segment. This model captures the key physical mechanisms that are responsible for the fluctuations of the fission chains.

We will use the parameter values given in Table I throughout this work.

### A. The critical regime

Nuclear reactors are operated at the critical regime, where the equilibrium between births by fission and deaths by capture allows the neutron population and hence the heat production to be stationary on average [3]. In our model, criticality is imposed by requiring that

$$\beta(\nu_{p,1} + \nu_{d,1} - 1) = \gamma, \quad (3)$$

which is equivalent to equating the production and disappearance rates. The criticality condition does not depend on the number of neutrons present in the system: indeed, nuclear reactors can be operated at steady-state at virtually any power level, the power being proportional to the average number of neutrons in the core. Due to its inherently stochastic nature, the neutron population density at a spatial site will display fluctuations (often dubbed

	$\theta = 1$	$\theta = 10^{-1}$	$\theta = 10^{-3}$
$N$	$10^2$	$10^2$	$10^2$
$M$	$10^2$	$10^3$	$10^5$
$L$	1	1	1
$\mathcal{D}$	$10^{-2}$	$10^{-2}$	$10^{-2}$
$\beta$	0.2	0.2	0.2
$\gamma$	0.3	0.3	0.3
$\lambda$	$10^{-1}$	$10^{-2}$	$10^{-4}$
$\nu_{p,1}$	2	2	2
$\nu_{d,1}$	0.5	0.5	0.5
$\nu_{p,2}$	2	2	2
$\nu_{d,2}$	0	0	0

TABLE I. Different sets of parameters used in this work. Here  $N$  is the initial (average) number of neutrons,  $M$  is the initial (average) number of precursors,  $L$  is the box half-size,  $\mathcal{D}$  is the diffusion coefficient,  $\beta$  is the fission rate,  $\gamma$  is the capture rate,  $\lambda$  is the decay rate of precursors,  $\nu_{p,l}$  and  $\nu_{d,l}$  are the  $l$ -th falling factorial moments of the number of neutrons and precursors produced from fission, respectively, and  $\theta = \lambda/(\beta\nu_{d,1})$ .

“neutron noise” [3]) because of random displacements in and out the spatial cell and because of random changes in the number of particles following fission and capture events within the cell.

### B. Observables of interest

Fluctuations are characterized by the statistical moments of the neutron population as a function of position and time. Let  $V_1$  and  $V_2$  be two non-overlapping detectors located within the reactor. We are interested in computing the average number of neutrons  $\mathbb{E}[n_i](t_i)$  and precursors  $\mathbb{E}[m_i](t_i)$  present at time  $t_i$  in detector  $i \in \{1, 2\}$ , and the two-point correlations between particles detected in  $V_1$  at time  $t_1$  and particles detected in  $V_2$  at time  $t_2$ , which stem from the cross-moments  $\mathbb{E}[n_1 n_2](t_1, t_2)$ ,  $\mathbb{E}[n_1 m_2](t_1, t_2)$ , and  $\mathbb{E}[m_1 m_2](t_1, t_2)$ . Often, it is preferable to work with continuous observables: we therefore define the neutron and precursor densities by taking the limits

$$n(x_i, t_i) = \lim_{V_i \rightarrow 0} \frac{\mathbb{E}[n_i](t_i)}{V_i} \quad (4)$$

$$m(x_i, t_i) = \lim_{V_i \rightarrow 0} \frac{\mathbb{E}[m_i](t_i)}{V_i}, \quad (5)$$

where  $x_i$  is the center of the detector location,  $i \in \{1, 2\}$ . The average population sizes are then obtained by integrating the particle densities over the entire system:

$$n(t) = \int n(x, t) dx \quad (6)$$

$$m(t) = \int m(x, t) dx. \quad (7)$$

Similarly, we define the pair correlation functions by taking the limits

$$u(x_1, t_1, x_2, t_2) = \lim_{V_1, V_2 \rightarrow 0} \frac{\mathbb{E}[n_1 n_2](t_1, t_2)}{V_1 V_2} \quad (8a)$$

$$v(x_1, t_1, x_2, t_2) = \lim_{V_1, V_2 \rightarrow 0} \frac{\mathbb{E}[n_1 m_2](t_1, t_2)}{V_1 V_2} \quad (8b)$$

$$w(x_1, t_1, x_2, t_2) = \lim_{V_1, V_2 \rightarrow 0} \frac{\mathbb{E}[m_1 m_2](t_1, t_2)}{V_1 V_2}. \quad (8c)$$

The function  $u(x_1, t_1, x_2, t_2)$  fully characterizes the behavior of fluctuations and correlations of the neutron population, and in this respect is key to the investigation of neutron noise. Similarly as for the case of the average densities, integral quantities can be obtained by integrating the previous equations over the whole spatial domain: for the two-point neutron correlation function, e.g., we would have

$$u(t_1, t_2) = \iint u(x, t_1, y, t_2) dx dy. \quad (9)$$

The information content of the two-point correlation function can be conveniently condensed in the *mean-squared neutron pair distance*  $\langle r^2 \rangle(t)$ , which is defined as

$$\langle r^2 \rangle(t) = \frac{\iint (x_1 - x_2)^2 u(x_1, t, x_2, t) dx_1 dx_2}{u(t, t)}, \quad (10)$$

which is also helpful in assessing the behaviour of neutron noise [21, 22]. In the following we will characterize the behaviour of these moments under different assumptions concerning the constraints imposed to the particle population.

### III. ANARCHIC MODEL

In the simplest incarnation of our model, we assume that the neutron and precursor populations are free to evolve according to the stochastic rules described in Sec. III, without any constraint. We will call this system the *anarchic* model (for illustration, see Fig. 1). The equations for the particle density and for the two-point correlation functions can be conveniently established using the backward master equation approach proposed by Pál and Bell (which is special case of Feynman-Kac backward formalism) [3, 6]. The idea is to first derive the equations for the moments  $n'_i(x_0, t_0) = n(x_i, t_i | x_0, t_0)$ , with  $i \in \{1, 2\}$ , and  $u'_{1,2}(x_0, t_0) = u(x_1, t_1, x_2, t_2 | x_0, t_0)$  conditioned to having a single initial neutron starting from position  $x_0$  at time  $t_0$ , treating  $x_1, x_2, t_1$  and  $t_2$  as parameters, and  $x_0$  and  $t_0$  as variables. The neutron density  $n'_i(x_0, t_0)$  is found to satisfy

$$\mathcal{L}^\dagger n'_i(x_0, t_0) = 0, \quad (11)$$

where we have introduced the adjoint linear operator

$$\begin{aligned} \mathcal{L}^\dagger f(x_0, t_0) &= \frac{\partial f}{\partial t_0} + \mathcal{D} \nabla_{x_0}^2 f + \alpha_p f \\ &+ \beta \nu_{d,1} \lambda \int_{t_0}^{\infty} f(x_0, t') e^{-\lambda(t'-t_0)} dt', \end{aligned} \quad (12)$$

with the shorthand

$$\alpha_p = \beta (\nu_{p,1} - 1) - \gamma. \quad (13)$$

As for the one-particle pair correlation function, we have

$$\begin{aligned} \mathcal{L}^\dagger u'_{1,2}(x_0, t_0) &= -\beta \nu_{p,2} n'_1(x_0, t_0) n'_2(x_0, t_0) \\ &- \beta \nu_{p,1} \nu_{d,1} \lambda n_1(x_0, t_0) \int_{t_0}^{t_2} e^{-\lambda(t'-t_0)} n'_2(x_0, t') dt' \\ &- \beta \nu_{p,1} \nu_{d,1} \lambda n_2(x_0, t_0) \int_{t_0}^{t_1} e^{-\lambda(t'-t_0)} n'_1(x_0, t') dt' \\ &- \beta \nu_{d,2} \lambda^2 \int_{t_0}^{t_1} \int_{t_0}^{t_2} e^{-\lambda(t'+t''-2t_0)} n'_1(x_0, t') n'_2(x_0, t'') dt' dt''. \end{aligned} \quad (14)$$

Equations (11) and (14) are linear and can be both solved in terms of the Green's function  $\mathcal{G}(x, t | x_0, t_0)$  associated to  $\mathcal{L}^\dagger$ . By separation of variables, the Green's function can be expressed as

$$\mathcal{G}(x, t, x_0, t_0) = \sum_{k=0}^{+\infty} \varphi_k(x) \varphi_k^\dagger(x_0) T_k(t | t_0), \quad (15)$$

where the time-eigenfunctions  $T_k(t | t_0)$  read

$$\begin{aligned} T_k(t | t_0) &= (\omega_k^+ - \omega_k^-)^{-1} \times \\ &\left[ e^{\omega_k^+(t-t_0)} (\omega_k^+ + \lambda) - e^{\omega_k^-(t-t_0)} (\omega_k^- + \lambda) \right], \end{aligned} \quad (16)$$

with two associated families of eigenvalues

$$\omega_k^\pm = \frac{\alpha_k + \alpha_p - \lambda \pm \sqrt{(\alpha_k + \alpha_p + \lambda)^2 + 4\lambda\beta\nu_{d,1}}}{2}. \quad (17)$$

The quantities  $\alpha_k$  are the eigenvalues associated to operator  $\mathcal{D} \nabla_x^2$ , with the corresponding eigenfunctions  $\varphi_k(x)$ . For reflection boundary conditions, we have  $\alpha_k = -\mathcal{D}(k\pi/2L)^2$  and

$$\varphi_k(x) = \cos\left(\frac{k\pi x}{2L}\right) \quad (18)$$

for  $k \geq 0$ . The functions  $\varphi_k^\dagger(x_0)$  are obtained from the orthonormality condition of the eigenfunctions, and for reflection boundary conditions read

$$\varphi_k^\dagger(x_0) = \begin{cases} \frac{1}{2L} & \text{if } k = 0 \\ \frac{1}{L} \cos\left(\frac{k\pi x_0}{2L}\right) & \text{if } k \geq 1. \end{cases} \quad (19)$$

In nuclear reactors, the two families  $\omega_k^\pm$  are widely separated because of the typical values of  $\lambda$ ,  $\alpha_p$  and  $\beta\nu_{d,1}$ . Loosely speaking, the  $\omega_k^+$  family is associated to the dynamics of precursors, while  $\omega_k^-$  describes prompt dynamics.

Once the single-particle moments are known, it is then straightforward to generalize the framework to describe a collection of  $\mathcal{N}$  *independent and identically distributed* individuals. The details of the calculations can be found in Appendix A. In particular, if we denote the single-particle source distribution as  $\mathcal{Q}(x_0, t_0)$ , the density  $n(x, t)$  reads

$$n(x, t) = \mathcal{N} \iint_{-\infty}^t \mathcal{Q}(x_0, t_0) \mathcal{G}(x, t|x_0, t_0) dx_0 dt_0, \quad (20)$$

which expresses a linear superposition principle. The pair correlation function can be also explicitly computed based on the Green's function, and reads

$$\begin{aligned} u(x_1, t_1, x_2, t_2) = & \\ & \frac{\mathcal{N} - 1}{\mathcal{N}} n(x_1, t_m) n(x_2, t_M) + \mathcal{G}(x_2, t_M|x_1, t_m) n(x_1, t_m) \\ & + \beta\nu_{p,2} \int_0^{t_m} \int \mathcal{G}(x_1, t_m|x, t) \mathcal{G}(x_2, t_M|x, t) n(x, t) dx dt \\ & + \beta\nu_{p,1}\nu_{d,1} \int_0^{t_m} \int \mathcal{G}(x_1, t_m|x, t) c(x_2, t_M|x, t) n(x, t) dx dt \\ & + \beta\nu_{p,1}\nu_{d,1} \int_0^{t_m} \int \mathcal{G}(x_2, t_M|x, t) c(x_1, t_m|x, t) n(x, t) dx dt \\ & + \beta\nu_{d,2} \int_0^{t_m} \int c(x_1, t_m|x, t) c(x_2, t_M|x, t) n(x, t) dx dt, \end{aligned} \quad (21)$$

where  $t_m = \min\{t_1, t_2\}$ ,  $t_M = \max\{t_1, t_2\}$ , and the quantity

$$c(x_1, t_1|x, t) = \lambda \int_t^{t_1} \mathcal{G}(x_1, t_1|x, t') e^{-\lambda(t'-t_1)} dt' \quad (22)$$

represents the expected number of neutrons detected at  $(x_1, t_1)$  produced by a precursor at  $(x, t)$ , with  $t_1 > t$ .

The terms appearing in the correlation function in Eq. (21) can be given a physical interpretation. The first term describes the contribution of the detection of uncorrelated particles, i.e. particles that do not share any common ancestor. The second term describes self-correlations, i.e. the detection of the same particle history at  $(x_1, t_m)$  and later at  $(x_2, t_M)$ . The four remaining terms represent the possible contributions due to fission events: the first one corresponds to the correlations induced by detection at  $(x_1, t_M)$  and  $(x_2, t_M)$  of neutrons stemming from different prompt neutrons produced by a common fission event at  $(x, t)$ ; the following two terms are symmetrical and correspond to correlations induced by detection at  $(x_1, t_M)$  and  $(x_2, t_M)$  of neutrons stemming from a prompt neutron and a precursor produced by a common fission event at  $(x, t)$ ; finally, the remaining

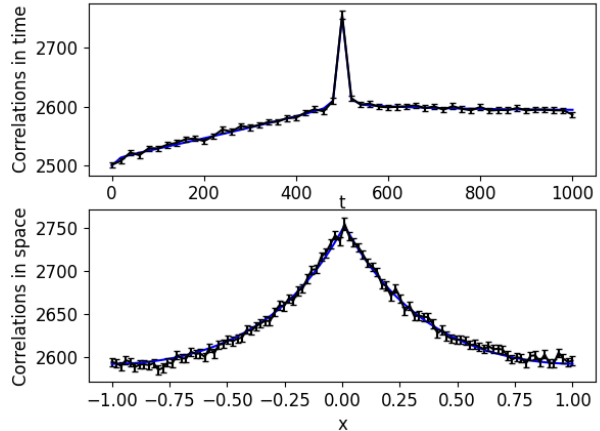


FIG. 2. Pair correlation function for a critical population starting with, on average,  $N = 100$  prompt neutrons and  $M = 10^3$  precursors, for a deterministic total population size  $\mathcal{N} = N + M$ . Parameters are taken as in Table I for  $\theta = 10^{-1}$ . On the graph we plot  $u(x_1, t_1, x_2, t)$  for  $x_1 = x_2 = 0$  and  $t_1 = T/2$ . The bottom graph shows  $u(x_1, t_1, x, t_2)$  the spatial shape when  $t_1 = t_2 = T$  and  $x_1 = 0$ . Blue: analytical results from Eq. (21). Black: Monte Carlo simulations result with  $10^6$  replicas.

term corresponds to correlations induced by detection at  $(x_1, t_M)$  and  $(x_2, t_M)$  of neutrons stemming from different precursors produced by a common fission event at  $(x, t)$ .

The reactor is assumed to be in the critical regime. It is then possible to choose the single-particle source  $\mathcal{Q}(x_0, t_0)$  so that the average neutron density  $n(x, t)$  is stationary at any time  $t > 0$ : this is for instance achieved by taking  $\mathcal{Q}(x_0, t_0) = \mathcal{Q}_c(x_0, t_0)$ , with

$$\mathcal{Q}_c(x_0, t_0) = \frac{1}{2L} \left[ \frac{\theta}{1+\theta} \delta(t_0) + \frac{1}{1+\theta} \lambda \exp(-\lambda t_0) \right], \quad (23)$$

where  $\theta = \lambda/(\beta\nu_{d,1})$ . Typically, for nuclear reactors,  $\theta \sim 10^{-4}$  to  $10^{-5}$ . This particular choice of  $\mathcal{Q}(x_0, t_0)$  will be called the *critical source*. The first term in Eq. (23) corresponds to neutrons appearing at  $t_0 = 0$  with probability  $\theta/(1+\theta)$ , while the second term corresponds to delayed neutrons appearing at exponentially distributed times from the decay of the precursors initially present at  $t_0 = 0$ , with complementary probability  $1/(1+\theta)$ . For our simple homogeneous one-dimensional reactor with reflection boundary conditions, the spatial distribution  $1/(2L)$  is flat over the domain (Eq. (18)).

### A. Analysis of the pair correlation function

Inspection of Eq. (20) shows that the average neutron density in a critical reactor starting from the critical

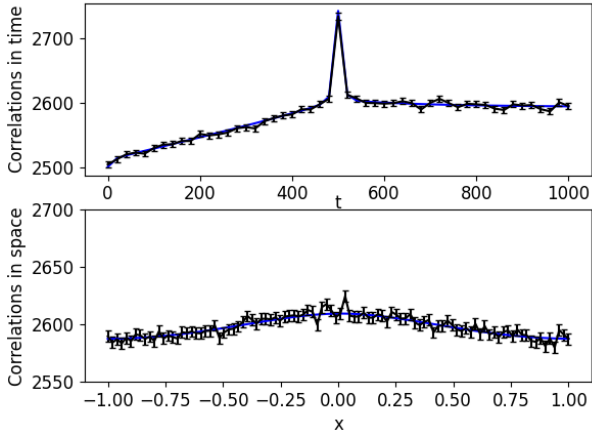


FIG. 3. Same as Fig. 2, except that the top graph gives the time dependency for  $x = 0$  and  $x_2 = -0.1$ . The bottom graph shows spatial correlations with  $t_1 = T = 990$  and  $t_2 = 1000$ .

source in Eq. (23) is trivially constant, as expected, and reads  $n(x, t) = N/(2L)$ . This value depends on the number  $N$  of neutrons emitted from the source and on the reactor size  $2L$ . Correspondingly, the average total number of neutrons  $n(t)$  will be constant and equal to  $N$ , and it can be shown that the average total number of precursors  $m(t)$  will be also constant and equal to  $M = N/\theta$ .

The correlation function in Eq. (21), on the contrary, is not stationary for a critical system. While Eq. (21) is exact, the evaluation of  $\mathcal{G}$  requires the numerical computation of an infinite series. In the following, the semi-analytical solution is henceforth obtained using Eqs. (B1-B11) by summing the series up to order  $k = 1000$ . The resulting correlation function has been carefully verified against Monte Carlo simulations, as shown in Figs. 2 and 3. It is more convenient to plot the *corrected pair correlation function*  $\tilde{u}(x_1, t_1, x_2, t_2) = u(x_1, t_1, x_2, t_2) - \delta(x_1 - x_2)n(x_1, t_1)$ , which is equivalent to ignoring the singular term  $\delta(x_1 - x_2)$  due to the self-correlations occurring in the system at  $t_1 = t_2$ . Note that this does not remove all of the self-correlation contributions, as self-correlations also include contributions from points  $x_1 \neq x_2$ . By abuse of language, and when it does not impede understanding, in the following we shall call  $\tilde{u}$  the “pair correlation function” nonetheless. Since the function has four independent variables, for the sake of simplicity we present one-dimensional cuts for fixed values of the other variables.

Figure 2 shows the time shape of the correlation function when particles are detected at the same spatial position  $x_1 = x_2$  (top panel), and the spatial shape when the detection times  $t_1 = t_2$  are the same (bottom panel). The detection positions chosen for Fig. 2 are far from the boundaries of the reactor. Figure 3 illustrates the time shape of the correlation function for two different detection positions (top), and its spatial shape for two

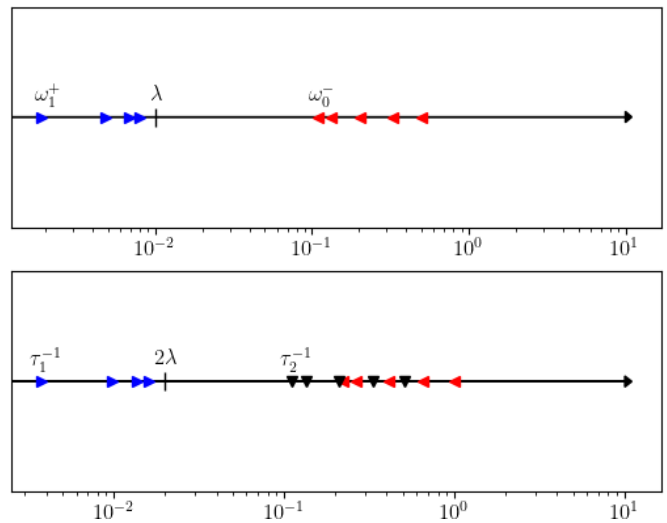


FIG. 4. Scatter plot of the characteristic time constants of the Green’s function (top) and of the one-time, two-point correlation function (bottom), for the anarchic system, up to order  $k = 5$ . Top: blue right-pointing triangles represent  $|\omega_k^+|$ ; red left-pointing triangles represent  $|\omega_k^-|$ . Bottom: blue right-pointing triangles represent  $|2\omega_k^+|$ ; black down-pointing triangles represent  $|\omega_k^+ + \omega_k^-|$ ; red left-pointing triangles represent  $|2\omega_k^-|$ . Note that  $\omega_0^- = 0$  and  $2\omega_0^- = 0$  cannot be represented in either plot (the system is critical). The dominant mode for each family ( $k = 0$ ) is the leftmost one. The parameter values are the same as in Fig. 2.

different detection times (bottom).

Figures 2 (top panel) and 3 (top panel) show that, after an initial transient,  $t \lesssim 50$ , the time profile of the pair correlation function exhibits a linear build-up. For  $t_1 > t_2$ , correlations saturate. Indeed, the linear build-up describes fissions happening at time  $t_1$  that may contribute to further fissions occurring at a fixed  $t_2$ , meaning that obviously fissions occurring at  $t_1 > t_2$  cannot contribute.

The analysis of  $u(x_1, t_1, x_2, t_2)$  shows that the correlation function displays several typical time scales. First, the spatial boundedness of the system introduces time scales that are related to diffusion. In the absence of delayed neutrons, the relaxation of the space profile of the correlation function is characterized by several time scales. The prompt time scales accumulate around and are asymptotically dominated by the mixing time, which is related to the time a neutron needs in order to explore the whole physical space [18]. With the introduction of precursors, additional remarkable time scales appear. As shown in Eq. (21), the two-point, two-time correlation function involves products of the Green’s function, Eq. (15), which has the structure of an infinite sum of exponential modes with characteristic time constants  $\omega_k^+$  and  $\omega_k^-$ . The correlation function can then be expressed as an infinite sum of exponential modes with characteristic time constants  $2\omega_k^+$ ,  $2\omega_k^-$ ,  $\omega_k^+ + \omega_k^-$  and  $\omega_k^+ - \omega_k^-$  (see Appendix B for details). If we restrict our

attention to the one-time, two-point correlation function,  $u(x_1, x_2, t) = u(x_1, t, x_2, t)$ , then the  $\omega_k^+ - \omega_k^-$  modes disappear. The first few characteristic time constants for each family are represented in Fig. 4. We can identify four different interesting time scales:

- the separation of the first two characteristic time constants of the  $\omega_k^+ + \omega_k^-$  family is given by  $(\omega_0^+ + \omega_0^-) - (\omega_1^+ + \omega_1^-) = -\alpha_1 = 4L^2/\mathcal{D}\pi^2 = \tau_D^{-1}$ . This is exactly the inverse of the mixing time for a system without delayed neutrons, as studied in Ref. 18. For the parameter values of Figs. 2 and 3, the prompt mixing time would be  $\tau_D \simeq 41$ .
- on a time scale of the order of  $\tau_2 = |\omega_0^+ + \omega_0^-|^{-1} = (\beta\nu_{d,1} + \lambda)^{-1}$ , the correlation function reaches a quasi-stationary regime, after prompt dynamics has stabilized but before delayed dynamics comes into play. Note that the expression of  $\tau_2$  is independent of the spatial characteristics of the system, such as its spatial extent or the diffusion coefficient. Therefore, this time scale corresponds to a collective behaviour. For times of the order of a few  $\tau_2$ , the prompt modes contribute a time-independent term to the correlation function. The delayed modes, on the other hand, have time scales that are much longer than  $\tau_2$ ; therefore, the remaining exponential terms  $\exp(2\omega_k^+ t)$  can be replaced with their first-order Maclaurin development, yielding a linear dependency on time. This explains the presence of linear build-up regimes in Figs. 2 and 3. For the parameters of these figures, we have  $\tau_2 \simeq 9$ .
- on a time scale of the order of  $\tau_1 = |2\omega_1^+|^{-1}$ , the correlation function acquires its asymptotic spatial shape. In this sense, this time scale is analogous to the mixing time of prompt systems; however, given the expression of Eq. (17), it involves the precursor decay constant  $\lambda$  and is therefore generally much longer than the prompt mixing time, which is given by  $\tau_D$ . For the parameter values of Figs. 2 and 3, we have  $\tau_1 \simeq 269$ .
- for times much longer than  $\tau_1$ , all the exponential terms in the correlation function have died out. The spatial shape of the correlation function is frozen, but the overall scale factor increases linearly with  $t$ . It has been previously shown by Houchmandzadeh et al. [19] (and our calculations confirm this) that the slope of this eventual linear regime is  $\tau_E^{-1}$ , where

$$\tau_E = \frac{N(1 + \theta)^2}{\beta\nu_2\theta^2}, \quad (24)$$

where

$$\nu_2 = \nu_{p,2} + 2\nu_{d,1}\nu_{p,1} + \nu_{d,2},$$

and  $N = \mathcal{N}\theta/(1 + \theta)$  is the average number of neutrons in the system. After a time of the order of

$\tau_E$ , the standard deviation of the total population size becomes equal to the mean population size. This is the regime of the critical catastrophe: because of the unbounded fluctuations, the population will almost surely go eventually extinct, despite the fact that the average population size is constant [3, 6]. This apparently paradoxical behaviour is a well-known characteristic of critical birth-and-death processes. The quantity  $\tau_E$  thus physically represents the typical *extinction time* of the system. For the parameter values of Figs. 2 and 3, the extinction time is  $\tau_E \simeq 1.5 \times 10^4$ ; therefore, this regime is not observable in the figures above.

The space profile of the correlation function, shown in Fig. 2 (bottom panel), has the tent-like shape that is typical of clustering behaviour. Despite the fact that the mean population density is uniform and constant, specific histories can exhibit strong patchiness (clusters) where pairs of particles will tend to be located at short distances from each other. This is coherent with previous findings for a reactor model neglecting delayed neutrons [18, 20, 23]. Figure 3 (bottom) suggests a relaxation toward a flat distribution for  $t_1$  and  $t_2$  sufficiently far from each another. Further analyses (not shown here for conciseness) confirm this conjecture.

It is tempting to characterize the importance of neutron clustering by defining a dimensionless parameter  $\eta = \tau_1/\tau_E$ , i.e. the ratio of the two longest time scales in the system. When  $\eta \gg 1$ , clustering will relax slowly over a time of the order of the extinction time, and therefore it will be observable over the whole lifetime of the system. It is interesting to consider how the dimensionless parameter  $\eta$  scales with  $\theta$  for small  $\theta$ , which is the regime of interest for nuclear reactors. By replacing  $\lambda = \theta\beta\nu_{d,1}$  in Eq. (17) and developing in Maclaurin series in  $\theta$ , we obtain

$$\omega_1^+ \simeq \frac{\theta}{\alpha_1^{-1} + \alpha_p^{-1}}. \quad (25)$$

Hence,

$$\tau_1 \simeq \frac{\alpha_1^{-1} + \alpha_p^{-1}}{2\theta}. \quad (26)$$

This should be contrasted with the mixing time for a system without delayed neutrons, which is  $\tau_D = 1/\alpha_1$ . Even in the regime where diffusion dominates ( $\alpha_1 \ll \alpha_p$ ), we can see that the presence of delayed neutrons slows down mixing by a factor of  $1/\theta$ . Unsurprisingly, this is the factor that is introduced by delayed neutrons in the characteristic response times of the *mean* reactor populations around criticality [19]. Thus, mixing is essentially a phenomenon that characterizes the behaviour of the average neutron and precursor densities.

When Eq. (26) is replaced in the definition of the clustering parameter  $\eta$ , we find

$$\eta = \frac{\tau_1}{\tau_E} \simeq \frac{\alpha_1^{-1} + \alpha_p^{-1}}{2N} \beta\nu_2\theta. \quad (27)$$



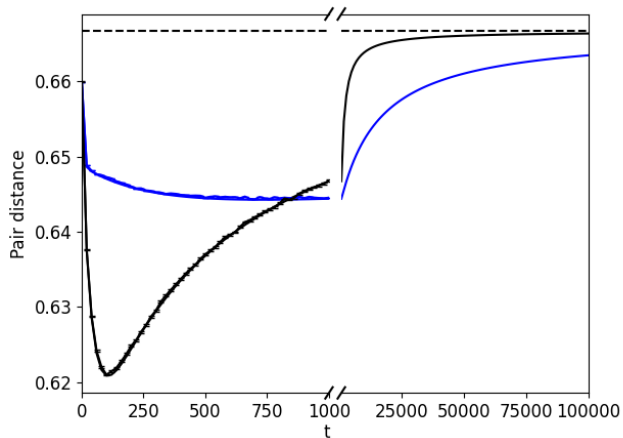


FIG. 5. Mean-squared pair distance in a one-dimensional box  $[-L, L]$  for critical populations using two sets of parameters taken from Table I. Error bars represent Monte Carlo simulation with  $10^6$  replicas, full lines the analytical integration of Eqs. (21) and (10). The blue curves correspond to  $\theta = 10^{-2}$ , and the black ones to  $\theta = 1$ .

This goes to show that the presence of delayed neutrons suppresses clustering, because of the different scaling of  $\tau_1$  and  $\tau_E$  with  $\theta$ . It is worth remarking in passing that the fact that the extinction time scales as  $\theta^{-2}$  for small values of  $\theta$  is not a coincidence, but it is due to the fact that  $\tau_E$  is a purely stochastic quantity, which can only be defined in terms of the second-order moments of the populations.

### B. Analysis of the mean-squared pair distance

The quantity  $\langle r^2 \rangle(t)$  yields the average square distance between pairs of particles (observed at the same time), and in this respect provides information on their tendency toward clustering [21, 22]. At time  $t_0 = 0$ , we have

$$\langle r^2 \rangle(0) = \langle r^2 \rangle_{iid} = \frac{2L^2}{3}, \quad (28)$$

since the neutrons are independently and uniformly distributed within the reactor. At later times, neutrons exhibit correlations induced by fission events and correspondingly  $\langle r^2 \rangle(t) < \langle r^2 \rangle_{iid}$ , which is a signature of the spatial clustering regime. For the anarchic model, we can obtain semi-analytical formulas for  $\langle r^2 \rangle(t)$  in the form of a series, whose expression can be found in Eq. (B13), generalizing previous findings for the model without delayed neutrons [21].

Figure 5 shows the time evolution of the mean-squared pair distance for a choice of model parameters. The formula from Eq. (B13) is compared to the result of the Monte Carlo simulation. Pair distance in Monte Carlo is estimated by taking the ensemble average of the squared

distances of all the neutron pairs present in the system at a given time, normalized by the ensemble average of the square of the number of particles at a given time. For times of the order of the extinction time, the quantity  $\langle r^2 \rangle(t)$  asymptotically reverts to the uncorrelated value  $\langle r^2 \rangle_{iid}$ , with a convergence speed that depends on the model parameters. This is explained by the fact that for  $t \gg \tau_E$  the population in a critical regime almost certainly dies out and correlations become spatially flat over the entire reactor. This result is again coherent with previous findings for the case where precursors were neglected [21].

## IV. MODELS WITH POPULATION CONTROL

So far, we have considered the case of freely evolving particle populations. In nuclear reactors, various feedback mechanisms act against the excursions of the neutron population. An example of utmost importance is provided by the Doppler effect. The probability of neutron-matter interaction depends on the temperature of the medium; in nominal conditions, the probability of sterile capture increases with increasing temperature [9]. Since the temperature of the reactor is driven by the number of neutrons in the system, the overall result of the Doppler effect is that deviations from the mean in the number of neutrons in the reactor tend to be quenched. The typical time scale of the Doppler effect is much shorter than the neutron lifetime, so that the feedback acts almost instantaneously on the behaviour of the fission chains [9].

For the model without delayed neutrons, these effects have been investigated by introducing an idealized control mechanism that acts as follows: whenever a neutron is created by fission, another neutron is randomly chosen and eliminated [20, 21]. This model was introduced based on heuristic arguments following previous works in the context of theoretical ecology [22, 24]: it preserves exactly the total number of individuals in the system and has a deep impact on the behaviour of the correlations. In particular, it has been shown to induce an upper bound on the amplitude of neutron noise and thus prevent the occurrence of the critical catastrophe [20, 21].

As a stepping stone towards a precise understanding of the effect of a physical feedback on the time and space shape of the correlation function, in the following we will introduce several simplified population control models that extend previous attempts by including precursors.

The rigorous derivation of the equations for the models with population control is provided in the Appendix C. The enforcement of control mechanisms, which correlate birth and death events, breaks the independence of particle histories, so that the backward formalism can hardly be used [25]. We will resort to a forward master equation approach instead. For the sake of simplicity, we will focus exclusively on the case of binary fission and on the production of at most one delayed neutron precursor, al-



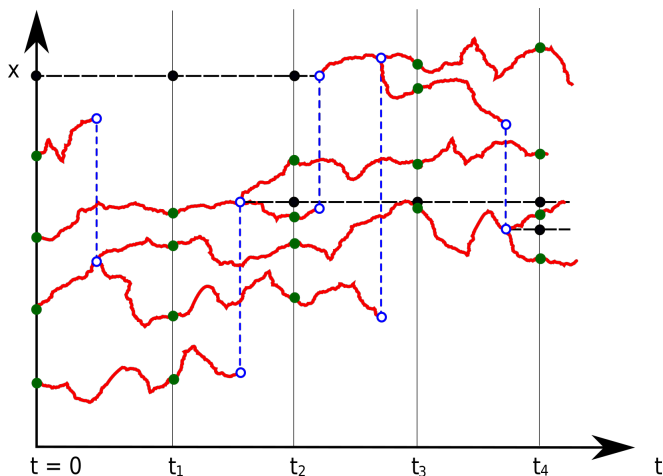


FIG. 6. A typical history for a system of 4 neutrons and 1 precursor in the  $N$ -control model. Neutrons diffuse (in red) until they branch or are destroyed by another neutron being produced in the system (these correlated event are shown in blue dashed lines), and precursor life-time is shown by black dashed-lines.

though our findings can be straightforwardly extended to general  $p_k$  and  $q_k$  distributions, at the expense of more cumbersome formulas. For the same reason, we shall take  $t_1 = t_2 = t$ , i.e. consider spatial correlations with both particles observed at the same time.

### A. Control of neutrons in a system of neutrons and precursors

Let us consider a population of neutrons and precursors, evolving based on the stochastic rules described in Sec. III. Since only neutrons are affected by physical feedback mechanisms (and are ultimately responsible for the physical changes occurring in the reactor), it would be natural to enforce population control on neutrons alone, which can be achieved as follows.

Each neutron induces fission with a rate of  $\beta$ ; the fission event produces exactly two prompt neutrons (with probability  $p_2 = 1$ ). Additionally, fission events produce a precursor with probability  $q_1$ , and no precursor with the complementary probability  $q_0 = 1 - q_1$ . Upon decay, with rate  $\lambda$ , the precursor yields a delayed neutron. In this specific case, we have  $q_1 = \nu_{d,1}$ , which is not true in general. In order to ensure a constant number  $N$  of neutrons in the system, whenever a neutron is produced, either from fission or from a decaying precursor, another neutron is randomly chosen and eliminated (for illustration, see Fig. 6). Observe that the total number of precursors is left free to fluctuate. We will call this scheme the  $N$ -control algorithm.

We begin our analysis by addressing the behaviour of the population sizes. First we denote by  $N$  and  $M$  the (arbitrary) initial number of neutrons and precursors, which we assume to be uniformly distributed in space.

From the forward master equation (see Appendix C for details), we deduce the equations for the average neutron and precursor population sizes, which read

$$\frac{\partial}{\partial t} n(t) = 0 \quad (29a)$$

$$\frac{\partial}{\partial t} m(t) = \beta \nu_{d,1} N - \lambda m(t). \quad (29b)$$

These equations can be readily solved, together with the initial conditions, and yield

$$n(t) = N$$

$$m(t) = \frac{\beta \nu_{d,1}}{\lambda} N (1 - e^{-\lambda t}) + M e^{-\lambda t}.$$

For the  $N$ -control model, the average total precursor number  $m(t)$  exponentially relaxes to the same equilibrium solution as for the anarchic model, i.e.,  $m_\infty = N \beta \nu_{d,1} / \lambda = N / \theta$ . If the initial condition is chosen as  $N = M \theta$ , we simply obtain  $m(t) = M$  for any  $t$ . The equations for the second-order moments of the total population can be also derived, and read

$$\frac{\partial}{\partial t} u(t) = 0 \quad (30a)$$

$$\frac{\partial}{\partial t} v(t) = \beta \nu_{d,1} u(t) - \lambda v(t) \quad (30b)$$

$$\frac{\partial}{\partial t} w(t) = \beta \nu_{d,1} N (2m(t) + 1) - \lambda (2w(t) - m(t)). \quad (30c)$$

The solutions to these equations are

$$u(t) = N^2 \quad (31)$$

$$v(t) = N m(t) \quad (32)$$

$$w(t) = m(t)^2 + m(t) - M e^{-2\lambda t}. \quad (33)$$

In the  $N$ -control model, the variance of the neutron population size is zero, as expected, which means in particular that the critical catastrophe is averted. The variance of the precursor population size converges exponentially to  $m_\infty$ . It is actually easy to show that the distribution of the precursor population size is asymptotically Poissonian, but we omit this proof for the sake of conciseness.

Starting from a fully spatially discretized master equation (see Appendix C), we can then obtain the equations for the spatial moments of the populations. The equations for the first moments read

$$\frac{\partial}{\partial t} n(x, t) = \mathcal{D} \nabla_x^2 n(x, t) + \lambda \left( m(x, t) - \frac{1}{N} H^n(x, t) \right) \quad (34a)$$

$$\frac{\partial}{\partial t} m(x, t) = \beta \nu_{d,1} n(x, t) - \lambda m(x, t), \quad (34b)$$

where we have defined the cross-moment

$$H^n(x, t) = \lim_{V_i \rightarrow 0} \frac{1}{V_i} \mathbb{E}[n_i(t) m(t)], \quad (35)$$

with  $V_i$  centered around  $x$ . A somewhat surprising fact is that the term  $H^n(x, t)$  appearing in the equation for the average is actually a second-order moment: this means that unfortunately the hierarchy of the spatial moment equations is not closed and analytical solutions are therefore out of reach for this model. This is to be contrasted with the case of the moments of the integral quantities, Eqs. (29) and (30), which are closed. On the other hand, Monte Carlo simulations show that, taking  $M = N/\theta$  and a uniform spatial distribution, then the first moments be-

have like in the anarchic case and verify

$$n(x, t) = \frac{N}{2L} \quad (36)$$

$$m(x, t) = \frac{M}{2L}. \quad (37)$$

Similarly, the equations for the pair correlation functions

$$\begin{aligned} \tilde{u}(x, y, t) &= u(x, t, y, t) - n(x, t)\delta(x - y) \\ v(x, y, t) &= v(x, t, y, t) \\ \tilde{w}(x, y, t) &= w(x, t, y, t) - m(x, t)\delta(x - y), \end{aligned}$$

involve third-order moments:

$$\begin{aligned} \frac{\partial}{\partial t} \tilde{u}(x, y, t) &= \mathcal{D}(\nabla_x^2 + \nabla_y^2) \tilde{u}(x, y, t) - \frac{2\beta}{N-1} \tilde{u}(x, y, t) + \lambda C_N (v(x, y, t) + v(y, x, t)) - \frac{2\lambda}{N} H^{nn}(x, y, t) \\ &\quad + \delta(x - y) \left( 2\beta n(x, t) + \frac{2\lambda}{N} H^n(x, t) \right) \end{aligned} \quad (38a)$$

$$\begin{aligned} \frac{\partial}{\partial t} v(x, y, t) &= \mathcal{D}\nabla_x^2 v(x, y, t) - \lambda C_N v(x, y, t) - \frac{\lambda}{N} H^{nm}(x, y, t) + \beta\nu_{d,1} C_{N-1} \tilde{u}(x, y, t) + \lambda \tilde{w}(x, y, t) \\ &\quad + \delta(x - y) \frac{\beta\nu_{d,1} N}{N-1} n(x, t) \end{aligned} \quad (38b)$$

$$\frac{\partial}{\partial t} \tilde{w}(x, y, t) = \beta\nu_{d,1} (v(x, y, t) + v(y, x, t)) - 2\lambda \tilde{w}(x, y, t). \quad (38c)$$

For the sake of brevity, we have defined the two third-order cross-moments

$$\begin{aligned} H^{nn}(x, y, t) &= \lim_{V_i, V_j \rightarrow 0} \frac{1}{V_i V_j} \mathbb{E}[n_i(t) n_j(t) m(t)] \\ H^{nm}(x, y, t) &= \lim_{V_i, V_j \rightarrow 0} \frac{1}{V_i V_j} \mathbb{E}[n_i(t) m_j(t) m(t)]. \end{aligned}$$

and the shorthand  $C_N = (N - 1)/N$ . The detection volumes  $V_i$  and  $V_j$  are assumed to be centered around  $x$  and  $y$ , respectively. It is interesting to notice that we can recognize in Eq. (38a) the *the renewal time* (or, equivalently, the fixation time [26])  $\tau_{R,0} = (N - 1)/(2\beta)$  for a population of prompt neutrons under population control without precursors [22]. In the absence of delayed neutrons, the renewal time is the typical time it takes for all surviving neutrons in the system to share the same common ancestor. Although this definition can be extended to a population of neutrons and precursors, we obviously expect the associated renewal time to differ from  $\tau_{R,0}$ .

On a side note, Monte Carlo simulations of the  $N$ -control model for  $\theta \ll 1$  seem to show that the relative spatial dependence of the pair correlation function is almost exactly the same as in the anarchic model for  $t_1 = t_2$ . This is illustrated in Fig. 7, where we plot the shape of the correlation function for both models, for a fixed value of  $y = -0.5$  and relative to its value in

$x = -L = -1$ . This remark does not hold true for  $\theta \sim 1$ .

Note that, although the hierarchy of the moment equations is not closed, the underlying stochastic process can be straightforwardly simulated using the Monte Carlo method. In the following, we shall make extensive use of this fact to compare the  $N$ -control model, which plays the role of a reference for population control, with other models enforcing similar constraints on the population. Indeed, the occurrence of  $H^{nn}(x, y, t)$  and  $H^{nm}(x, y, t)$  suggests that the lack of closure originates from the fact that the  $N$ -control model correlates the size of the precursor population with the local neutron and precursor densities. It is tempting to suggest the use of the approximation

$$H^n(x, t) \simeq n(x, t)m(t) \quad (39)$$

in order to close Eqs. (34), and of similar approximations for  $H^{nn}(x, y, t)$  and  $H^{nm}(x, y, t)$ . Doing so in the general case yields equations with time-dependent coefficients in the moment equations. However, we do not know how to construct a Monte Carlo game associated to these approximate moment equations. This effectively prevents us from comparing the analytical results that we would eventually obtain with the corresponding simulation results.

Another way to close the hierarchy of moment equations is to apply population control to both populations,

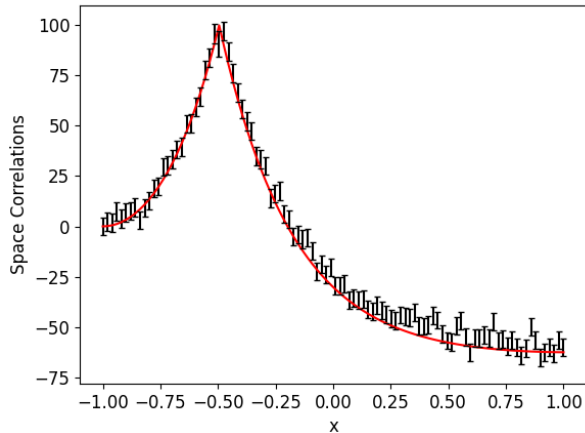


FIG. 7. Spatial dependence of the difference between the pair correlation function evaluated in  $(x, y = -0.5)$  and  $(x = -L = -1, y = -0.5)$ . The black curve is given by a Monte Carlo simulation of the  $N$ -control scheme, while the red one is given by the analytical solution of the anarchic model. Here,  $\theta = 10^{-3}$ . Parameters are taken from Table I.

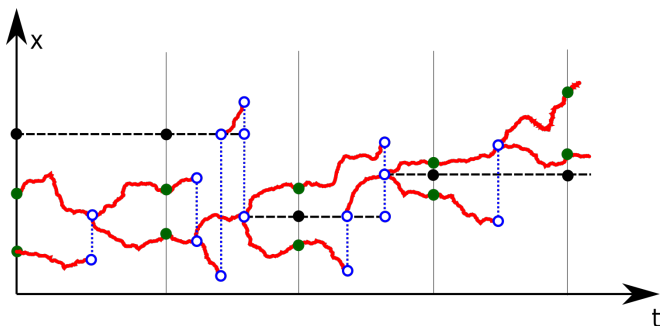


FIG. 8. A typical history for a system of 2 neutrons and 1 precursor in the  $NM$ -control model. Neutrons diffuse (in red) until they branch or are destroyed by another neutron being produced in the system (these correlated event are shown in blue dashed lines), and precursor life-time is shown by black dashed-lines.

so that the size of the precursor population is not a random variable. By doing so, we sacrifice some of the physical relevance of the  $N$ -control model, but we gain the ability to derive analytical solutions while keeping an exact associated Monte Carlo game. We henceforth propose two alternative models and we discuss under which con-

ditions they may satisfyingly approximate the  $N$ -control model.

## B. Control of neutrons and precursors

Let us now consider a process in which the total number of neutrons  $N$  and the total number of precursors  $M$  are kept under constraint. Conservation of  $N$  is enforced as previously described. Conservation of  $M$  is enforced as follows: when a neutron undergoes fission and produces a precursor, another randomly chosen precursor is destroyed. When a precursor emits a delayed neutron, the precursor is *not* destroyed. In this way, we ensure that  $N$  and  $M$  are kept constant at any time (see Fig. 8). We call this algorithm the  $NM$ -control scheme.

For the total population statistics,  $NM$ -control trivially yields one possible state, given by the initial condition  $(N, M)$ , with vanishing variance. It appears however that the spatial behaviour is non-trivial. Additionally, direct calculation confirms that the constraint of fixed  $(N, M)$  indeed sidesteps the closure issues of the  $N$ -control model. The equations for the first-order moments are now closed and read:

$$\frac{\partial}{\partial t} n(x, t) = \mathcal{D} \nabla_x^2 n(x, t) + \lambda \left( m(x, t) - n(x, t) \frac{M}{N} \right) \quad (40a)$$

$$\frac{\partial}{\partial t} m(x, t) = \beta \nu_{d,1} \left( n(x, t) - m(x, t) \frac{N}{M} \right). \quad (40b)$$

If  $N$  and  $M$  are in the equilibrium ratio  $N/M = \theta = \lambda/(\beta \nu_{d,1})$ , then Eqs. (40) reduce to the usual forward equations for the first moments of freely evolving populations of neutrons and precursors [19]. This has two consequences. First, we can conclude that the mixing time for the  $NM$ -control model is the same as for the anarchic model,  $\tau_1$ . Second, Eqs. (40) admit uniform and constant asymptotic solutions

$$n(x, t) \rightarrow n_\infty(x) = \frac{N}{2L} \quad (41a)$$

$$m(x, t) \rightarrow m_\infty(x) = \frac{M}{2L}. \quad (41b)$$

For the second-order moments we obtain once again a closed system of equations:

$$\begin{aligned} \frac{\partial}{\partial t} \tilde{u}(x, y, t) &= \mathcal{D} (\nabla_x^2 + \nabla_y^2) \tilde{u}(x, y, t) - \tau_n^{-1} \tilde{u}(x, y, t) + \lambda C_N (v(x, y, t) + v(y, x, t)) \\ &\quad + 2\beta\delta(x-y)n(x, t) \end{aligned} \quad (42a)$$

$$\begin{aligned} \frac{\partial}{\partial t} v(x, y, t) &= \mathcal{D} \nabla_x^2 v(x, y, t) - \tau_c^{-1} v(x, y, t) + \beta\nu_{d,1} C_{N-1} \tilde{u}(x, y, t) + \lambda \tilde{w}(x, y, t) \\ &\quad + \delta(x-y) (2\beta\nu_{d,1} n(x, t) + \lambda m(x, t)) \end{aligned} \quad (42b)$$

$$\frac{\partial}{\partial t} \tilde{w}(x, y, t) = \beta\nu_{d,1} C_M (v(x, y, t) + v(y, x, t)) - \tau_p^{-1} \tilde{w}(x, y, t). \quad (42c)$$

with  $C_M = (M-1)/M$  and where we defined the time constants

$$\tau_n = \left( \frac{2\beta}{N-1} + \frac{2\lambda M}{N} \right)^{-1} \quad (43a)$$

$$\tau_c = \left( \frac{\beta\nu_{d,1}N}{M} + \lambda \frac{M}{N} \right)^{-1} \quad (43b)$$

$$\tau_p = \frac{M}{2\beta\nu_{d,1}N}, \quad (43c)$$

Equations (42) are a linear system of equations for  $(\tilde{u}, v, \tilde{w})$ . Following the heuristic arguments of Zhang et al. [24], we should expect the renewal time for our system to be determined by the dominant time constant of the correlation functions. In the  $NM$ -control model, the collective modes of the correlation functions are associated to the eigenvalues of the matrix of the coefficients of  $(\tilde{u}, v, \tilde{w})$  in Eqs. (42), which reads

$$R = \begin{pmatrix} -\tau_n^{-1} & 2\lambda C_N & 0 \\ \beta\nu_{d,1} C_{N-1} & -\tau_c^{-1} & \lambda \\ 0 & 2\beta\nu_{d,1} C_M & -\tau_p^{-1} \end{pmatrix}. \quad (44)$$

Assuming that  $N$  and  $M$  are chosen in the equilibrium ratio  $N = \theta M$  and that  $N$  is large, we can extract the scaling behaviour of the eigenvalues of  $R$  with respect to  $\theta$ , for small  $\theta$ . The eigenvalues  $\{r_1, r_2, r_3\}$  read

$$r_1 \simeq -2\beta\nu_{d,1} \quad (45)$$

$$r_2 \simeq -\beta\nu_{d,1} \quad (46)$$

$$r_3 \simeq -\frac{2\beta\theta^2(1+3\nu_{d,1})}{N(1+\theta)^2}, \quad (47)$$

with  $r_1 < r_2 < r_3$ . The time constant associated to the dominant eigenvalue,  $r_3$ , is the renewal time for the  $NM$ -control model, and reads

$$\tau_R^{NM} \simeq \frac{N(1+\theta)^2}{2\beta\theta^2(1+3\nu_{d,1})}. \quad (48)$$

This expression is very similar to the extinction time for the anarchic scheme, Eq. (24). However, the renewal time  $\tau_R^{NM}$  is not related to the extinction time for the system, because no critical catastrophe is possible in the  $NM$ -control model.

As we did for the anarchic scheme, we can then define a dimensionless clustering parameter  $\eta^{NM} = \tau_1/\tau_R^{NM}$ . However, given that the mixing time of the  $NM$ -control scheme is the same as the mixing time of the anarchic scheme, and that the renewal time  $\tau_R^{NM}$  is very similar to the extinction time of the anarchic scheme, the clustering parameter also results in a  $1/\theta$  scaling for small  $\theta$ , and the remarks made about the anarchic scheme apply verbatim to the  $NM$ -control scheme.

The full solution for Eqs. (42) is cumbersome. However, we can obtain asymptotic solutions in the form of Fourier series. Let  $\tilde{u}_\infty(x, y)$ ,  $v_\infty(x, y)$  and  $\tilde{w}_\infty(x, y)$  be the asymptotic shapes of the correlation functions for long times:

$$\begin{aligned} \tilde{u}_\infty(x, y) &= \lim_{t \rightarrow \infty} \tilde{u}(x, y, t) \\ v_\infty(x, y) &= \lim_{t \rightarrow \infty} v(x, y, t) \\ \tilde{w}_\infty(x, y) &= \lim_{t \rightarrow \infty} \tilde{w}(x, y, t). \end{aligned}$$

We use the following Fourier decomposition:

$$f(x, y) = \sum_{k_x, k_y = -\infty}^{+\infty} f_{k_x, k_y} \exp(i\kappa_{k_x} x) \exp(i\kappa_{k_y} y). \quad (49)$$

Here  $\kappa_k = k\pi/(2L)$  are the characteristic wave numbers for reflection boundary conditions and  $f(x, y)$  stands for any of  $\tilde{u}_\infty(x, y)$ ,  $v_\infty(x, y)$  or  $\tilde{w}_\infty(x, y)$ . The coefficients satisfy the relation

$$f_{k_x, k_y} = \frac{1}{2\pi} \iint \exp(-i\kappa_{k_x} x) \exp(-i\kappa_{k_y} y) f(x, y) dx dy. \quad (50)$$

The linear system of equations solved by the Fourier coefficients can be obtained from Eqs. (42) by setting the time derivative terms to zero, multiplying by  $\exp(-i\kappa_{k_x} x) \exp(-i\kappa_{k_y} y)/(2\pi)$ , integrating over  $dx dy$  and using Eq. (50) and Eqs. (40). The analytical expressions of the coefficients are given in Eqs. (D3).

The asymptotic two-point neutron-neutron correlation function for the  $NM$ -control model was numerically computed by truncating the Fourier series after 1000 terms.

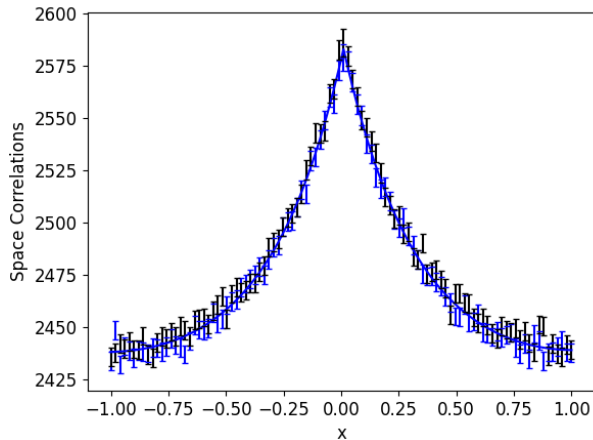


FIG. 9. Asymptotic pair correlation function for  $\theta = 10^{-3}$  and  $y = 0$ . The parameters are taken from Table I. Black line: analytical solution of the  $NM$ -control scheme, Eqs. (42). Black with error bars: Monte Carlo simulations for the  $N$ -control scheme. Blue with error bar: Monte Carlo simulations of the  $NM$ -control scheme, both with  $10^6$  replicas.

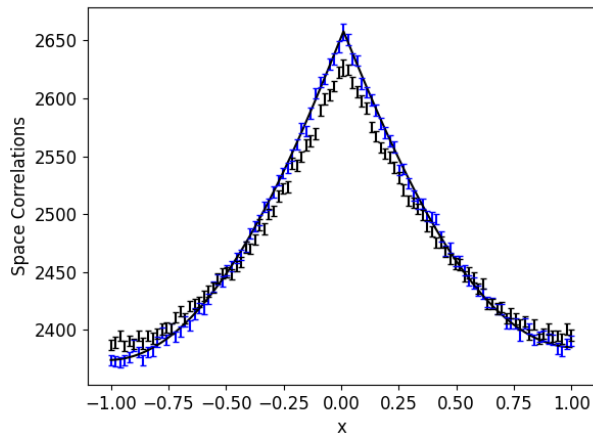


FIG. 10. Same color code as Fig. 9 but the parameters are taken from Table I for  $\theta = 1$ .

It is compared with Monte Carlo simulations for the  $N$ -control and the  $NM$ -control scheme, for two sets of physical parameters, in Figs. 9 and 10.

For  $\theta = 0.001$  (Fig. 9), the  $NM$ -control scheme provides a good approximation of the  $N$ -control scheme, and all the curves representing neutron correlations are very similar. This means that, when  $\theta \ll 1$ , which is the case in nuclear reactors, a system where neutrons and precursors are both kept under control has similar correlation functions as a system where population control acts on neutrons alone. On the other hand, when  $\theta = 1$  (Fig. 10), the  $N$ -control and  $NM$ -control models yield similar, but different correlation functions. Indeed, we observe that the  $NM$ -control scheme results

in stronger spatial short-range correlations compared to the  $N$ -control scheme, while long-range correlations are weaker in the  $NM$ -control scheme. This can be easily explained: in the  $N$ -control scheme, when a precursor decays, it is destroyed and replaced by a neutron that immediately starts diffusing. This mechanism can be seen as a kind of delayed diffusion; when a neutron induces a fission event and produces a precursor, it effectively suspends diffusion for a time of the order of  $1/\lambda$ . On the other hand, in the  $NM$ -control model, a precursor does not die when it decays, and thus plays the role of a source at a fixed position until it is replaced by another precursor. The precursor density can then undergo significant local fluctuations favouring short-range correlations by inducing overproduction of neutrons in a small volume, at the expense of long-range correlations.

Some insight about the similarity between the  $N$ -control and  $NM$ -control schemes for  $\theta \ll 1$  can be gained by comparing Eqs. (38) and Eqs. (42). Indeed, remember that  $\theta \ll 1$  means that the number of precursors is much larger than the number of neutrons. If  $m(t)$  is sufficiently large, which is the case here, its fluctuations will be negligible compared to its mean value. This allows us to consider  $m(t)$  as a deterministic observable. If we then assume that

$$\mathbb{E}[n_i(t)n_j(t)m(t)] \simeq \mathbb{E}[n_i(t)n_j(t)]\mathbb{E}[m(t)],$$

then Eq. (38a) reduces to Eq. (42a). Thus, in this limit, neutron-neutron correlations follow the same dynamics in both schemes. It is worth remarking however that, under the same approximation, the equations for  $v$  and  $\tilde{w}$  in the  $N$ -control model do not reduce to the corresponding equations in the  $NM$ -control model.

### C. Immigration model

We have observed that the precursor population only exhibits weak fluctuations in the  $\theta \ll 1$  limit. This suggests an alternative model where precursors are modeled as a fixed external source, with the aim of obtaining a time-dependent solution that, in this limit, successfully approximates the  $N$ -control model. Thus, we model the system as a collection of neutrons under population control, with an external, time-independent source term modelling precursor decay. Formally, this model is equivalent to an *immigration model* with a time-independent, Poissonian immigration source describing the asymptotic precursor decay density, given by

$$\mathcal{Q}_I(x) = \lambda m_\infty(x) = \frac{\lambda}{\theta} n_\infty(x), \quad (51)$$

where  $\theta$  is the parameter of the equivalent  $NM$ -control scheme. Population control is enforced by requiring that each time a new neutron enters the system, whether by fission or from the external source, we destroy another randomly chosen neutron, as illustrated in Fig. 11.

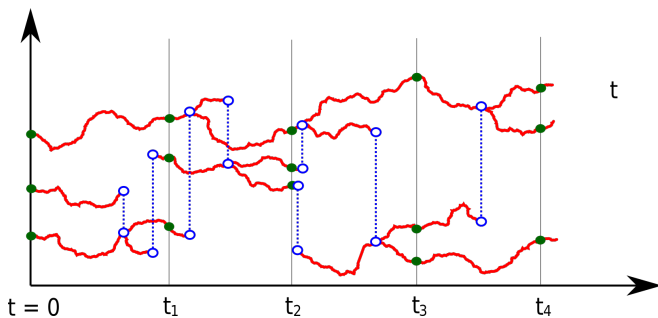


FIG. 11. A typical history for a system with 3 neutrons at  $t = 0$ , in the immigration model. Neutrons diffuse (in red) until they branch or are killed by another neutron branching somewhere else (blue lines show these correlated events). They can also be produced by the source, thus killing another randomly chosen neutron.

Following the usual derivation method, we obtain the equation for the average neutron density, namely

$$\frac{\partial}{\partial t} n(x, t) = \mathcal{D} \nabla^2 n(x, t) - \frac{\lambda}{\theta} n(x, t) + \mathcal{Q}_I(x). \quad (52)$$

Taking  $\mathcal{Q}_I(x)$  as given by Eq. (51), the last two terms asymptotically cancel out and the dynamics of the average is driven only by diffusion, similarly to what happens in the anarchic model when the system is critical.

The equation for the pair correlation function reads

$$\begin{aligned} \frac{\partial}{\partial t} \tilde{u}(x, y, t) = & \mathcal{D} (\nabla_x^2 + \nabla_y^2) \tilde{u}(x, y, t) - \tau_n^{-1} \tilde{u}(x, y, t) \\ & + C_N (n(x, t) \mathcal{Q}_I(y) + n(y, t) \mathcal{Q}_I(x)) \\ & + 2\beta \delta(x - y) n(x, t), \end{aligned} \quad (53)$$

where we recognize  $\tau_n$  from Eq. (43a). Thus, in this model, neutron pair correlations relax with a time constant governed by  $\tau_n$ .

Equations (52) and (53) have the same form as Eqs. (40a) and (42a), provided that one replaces  $\mathcal{Q}_I(x)$  by its expression, Eq. (51). These equations can be solved analytically. In particular, taking a uniform initial condition for  $n(x, t)$ , we obtain

$$n(x, t) = \frac{N}{2L} \quad (54)$$

for the average neutron density, and

$$\begin{aligned} \tilde{u}(x, y, t) = & \frac{N(N-1)}{4L^2} \exp\left(-\frac{t}{\tau_n}\right) \\ & + \frac{2\tau_n \lambda M(N-1)}{4L^2} \left[ 1 - \exp\left(-\frac{t}{\tau_n}\right) \right] \\ & + \frac{2\beta N}{2L} \int dx' \int_0^t dt' \mathcal{G}'(x, t|x', t') \mathcal{G}'(y, t|x', t') \\ & \exp\left(-\frac{t-t'}{\tau_n}\right) \end{aligned} \quad (55)$$

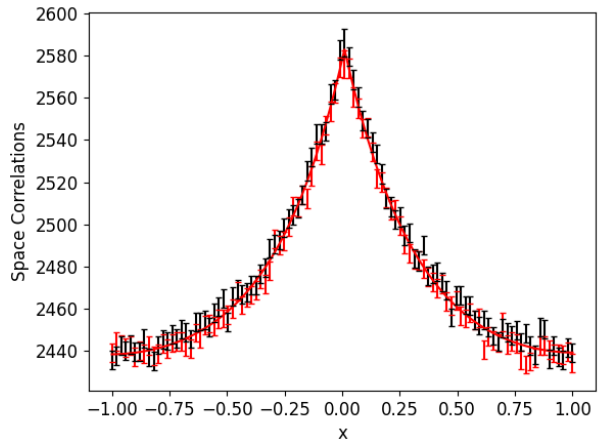


FIG. 12. Asymptotic pair correlation function for  $\theta = 0.001$  and  $y = 0$ . Parameters are the same as in Fig. 9. Red curve: analytical solution of the immigration model. Red error bars: Monte Carlo simulations of the immigration model. For reference, the results of the  $N$ -control scheme are plotted in black.

for the pair correlation function, where  $\mathcal{G}'$  is the Green's function associated to Eq. (52). As a side note, taking the  $\lambda \rightarrow 0$  limit in this equation we recover the pair correlation function for a system of prompt neutrons under population control [18, 20, 22].

Comparison with Monte Carlo simulations (see Fig. 12) shows that, for systems where  $\theta \ll 1$ , the immigration model closely matches the  $N$ -control model; the remarks made about Fig. 7 also apply to the immigration model. Figure 13 provides the same comparison for a larger value of  $\theta$ . Comparing Fig. 13 and Fig. 10, it is clear that the  $N$ -control model is better approximated by the  $NM$ -control model than by the immigration model. This is unsurprising, in view of the crudeness of the treatment of neutron-precursor correlations in the immigration model.

To summarize the results of this section, we have modeled feedback as an idealized mechanism enforcing strict conservation of the total number of neutrons. We showed that doing so raises a problem of non-closure of the associated hierarchy of moment equations. Enforcing population control on neutrons and precursors solves the closure problem, but results in a less physically realistic model, especially if the condition  $\theta \ll 1$  does not hold. We also showed that it is possible to model precursors as a fixed source term related to the asymptotic precursor density, which also results in a satisfactory approximation of the neutron-precursor model for  $\theta \ll 1$ .

#### D. Mean-squared pair distance functions

We now discuss the mean-squared pair distance for our population control models, and we compare it to the case of an anarchic population.



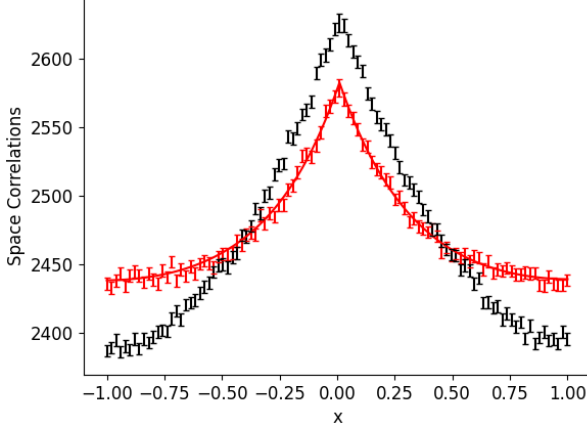


FIG. 13. Same color code than Fig. 12, and parameters corresponding to  $\theta = 1$  in Table I.

For the  $N$ -control scheme, we do not have access to an analytical expression for the mean-squared pair distance, because the moment equations, Eqs. (38), are not closed. However, we do have an asymptotic correlation function for the  $NM$ -control scheme, given by Eqs. (D3), from which we can deduce an asymptotic mean-squared pair distance. For reflection boundary conditions, it is given by

$$\langle r_{NM}^2 \rangle = \frac{8L^4 \tilde{u}_{0,0}}{3N^2} - \left( \frac{16L^2}{\pi^2 N} \right)^2 \sum_{k=1}^{+\infty} \frac{\tilde{u}_{k,k}}{k^4}, \quad (56)$$

where  $\tilde{u}_{k,k}$  is the Fourier coefficient for the neutron-neutron correlations asymptotic solution of Eq. (42a). On physical grounds, we expect the asymptotic pair distance in the  $NM$ -control scheme to be always smaller than the uncorrelated value, Eq. (28).

As for the immigration model, an analytical expression for the mean-squared pair distance can be obtained by applying the definition of the mean-squared pair distance function, Eq. (10), to the solution, Eq. (55). For reflection boundary conditions, straightforward calculations hence yield

$$\langle r_I^2 \rangle(t) = C_N \frac{2L^2}{3} - \frac{128L^2 \beta}{N} \sum_{k=1}^{+\infty} \frac{1 - e^{-(\tau_n^{-1} - 2\alpha_k)t}}{(k\pi)^4 (\tau_n^{-1} - 2\alpha_k)} \quad (57)$$

The sum can be computed analytically in the asymptotic limit and reads

$$\langle r_I^2 \rangle_{\infty} = C_N \frac{2L^2}{3} + \frac{16\beta\tau_n}{N} \times \left( \left( \frac{D\tau_n}{L} \right)^2 - \frac{2D\tau_n}{3} - \frac{4L^2}{45} - \frac{\sqrt{2}(D\tau_n)^{\frac{3}{2}}}{L} \cot \sqrt{\frac{2\tau_n}{D}} L \right) \quad (58)$$

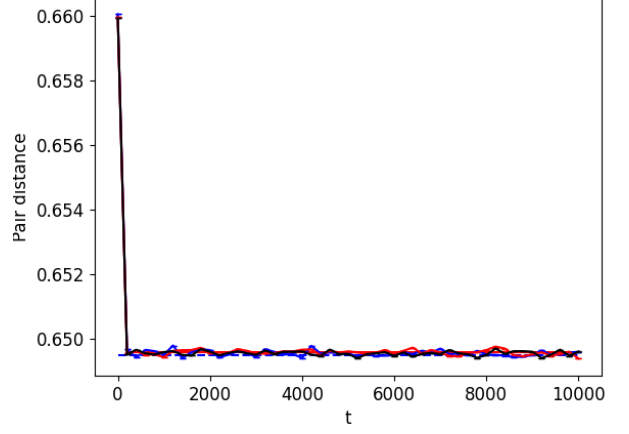


FIG. 14. Mean-squared pair distance for the same parameters as Fig. 9 ( $\theta = 0.001$ ). Blue dashed line:  $NM$ -control model analytical asymptotic value; blue with error bar: Monte Carlo result; red dashed line: immigration model analytical solution; red with error bar: Monte Carlo result; black:  $N$ -control model Monte Carlo result. All simulation results are obtained with  $10^6$  replicas.

If we take the mean-squared pair distance as an indicator of clustering, Fig. 14 clearly illustrates that the three models have very similar clustering behaviour for  $\theta \ll 1$ , even for very long times. For  $\theta \sim 1$ , on the other hand, the models behave differently, as shown in Fig. 15. In particular, we note that the immigration model yields the largest mean-squared pair distance of all the considered control schemes. This is easily explained by the fact that the “decay source” of the immigration model is assumed to be uniformly distributed in space and completely uncorrelated with the neutrons, an assumption that is bound to reduce clustering. The  $NM$ -control scheme yields a smaller mean-squared pair distance than the  $N$ -control scheme, indicating that clustering is more prominent in the former. This behavior can be explained by observing that a precursor may in fact produce several neutrons at the same position before being destroyed, which tends to increase clustering. It is interesting to note that for all control models the squared pair distance asymptotically converges to  $\langle r^2 \rangle_{\infty} < \langle r^2 \rangle_{iid}$ , because the critical catastrophe is avoided, contrary to what happens in the anarchic case. However, Eqs. (56) and (58) show that  $\langle r^2 \rangle_{\infty}$  tends to the uncorrelated value as  $N$  tends to infinity.

## V. CONCLUSIONS

We considered a simplified one-dimensional model of a nuclear reactor including neutrons and precursors. We derived moment equations characterizing the spatial correlations of our system. Our main tool was the two-point, two-time neutron-neutron second-order moment (here-



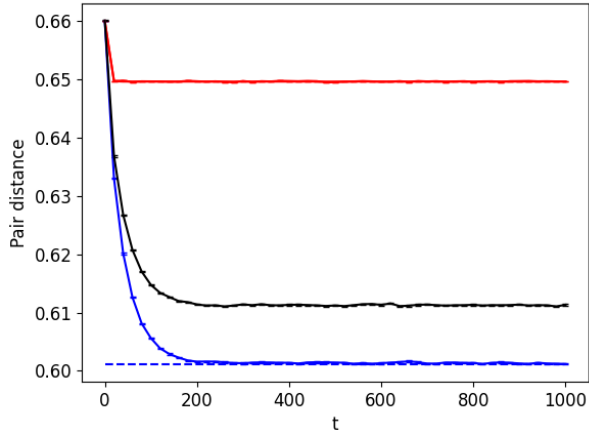


FIG. 15. Mean-squared pair distance with same parameters as in Fig. 10 ( $\theta = 1$ ), and color code of Fig. 14.

after named pair correlation function), which characterizes the joint observation of neutrons at  $(x_1, t_1)$  and at  $(x_2, t_2)$ . By using the Pál and Bell backward formalism, we derived the pair correlation function for the anarchic model, where all the populations are left free to evolve. We identified two typical time scales, namely the time  $\tau_2$  necessary for the prompt correlation dynamics to relax, and the time  $\tau_1$  necessary for correlations to achieve their asymptotic spatial shape. The latter generalizes the concept of mixing time to a system with delayed neutrons; however, for typical values of the physical parameters,  $\tau_1$  is actually much longer than the mixing time of a critical system without delayed neutrons. The system is furthermore characterized by its extinction time  $\tau_E$ , which represents the typical time required to observe catastrophic fluctuations of the total population size. Similarly to the mixing time, the extinction time for a system with delayed neutrons is much longer than the extinction time for a critical system without delayed neutrons, for typical values of the physical parameters.

In an attempt to take into account feedback effects, we introduced several idealized population control mechanisms. These models break the statistical independence of the neutron fission chains, which forced us to abandon the Pál and Bell backward formalism in favor of the

forward formalism. We derived the master equations for three different population control models:

- in the  $N$ -control model, the neutron population is kept constant, but no constraint is applied to the precursor population. This model yields a non-closed hierarchy of moment equations;
- in the  $NM$ -control model, both the neutron and precursor populations are controlled. This model yields a closed hierarchy of moment equations. We identified the dominant time scales of the model and presented asymptotic solutions for the first two moment orders.
- in the immigration model, precursors are modeled as a uniform Poisson neutron source whose intensity is equal to the asymptotic precursor decay rate at equilibrium.

For each model, we obtained two-point, one-time pair correlation functions by Monte Carlo simulations, and by analytical means when possible. Comparisons between analytical solutions and Monte Carlo simulations showed that all the models yield very close results when  $\theta \ll 1$ , which is the main regime of interest for nuclear reactors. We also showed that the introduction of population control prevents the occurrence of the critical catastrophe and thus quenches clustering.

As a prospect for future work, it is of course interesting to consider the possibility of lifting the simplifying assumptions of our current model, e.g. by introducing energy- and space-dependent neutron interaction rates, and by replacing the diffusion approximation (Brownian motion) with transport (jump processes with random redistribution of directions). These refinements, however, would probably bring the models out of reach of an analytical treatment. More interestingly, population control acts as a global mechanism in our model, whereas in reality feedback effects are local. This suggests the study of spatially-dependent versions of the population control mechanisms considered here. Finally, the extension of the present work to non-critical regimes is relevant to reactors in power excursions (e.g., during start-up and shut-down), and is also particularly interesting for ecological, epidemiological and biological models.

## Appendix A: Backward formalism for the anarchic model

Consider the branching Brownian motion whose stochastic rules are given in Sec. III and assume that no constraint is enforced on the total population. Let  $V_1$  and  $V_2$  be two finite-size non-overlapping detectors, and let  $\mathcal{P}(n_1, t_1, n_2, t_2 | x_0, t_0)$  be the probability to find  $n_1$  particles at time  $t_1$  in detector  $V_1$  and  $n_2$  particles at time  $t_2$  in detector  $V_2$ , for a single particle starting in  $x_0$  at time  $t_0$ , with  $t_2 > t_1$ ; the results for  $t_2 < t_1$  are recovered by arguments of symmetry. Pál and Bell have independently derived a backward formalism yielding the (adjoint) master equation for  $\mathcal{P}$ . The manipulation of the resulting equation is rather cumbersome, and in most cases neutron noise can be characterized using the lowest-order moments of  $n_1$  and  $n_2$ . We will be in particular interested in the average

number of neutrons in detector  $V_1$  at time  $t_1$ , namely,

$$\mathbb{E}[n_1](t_1|x_0, t_0) = \sum_{n_1, n_2} n_1 \mathcal{P}(n_1, t_1, n_2, t_2|x_0, t_0) \quad (\text{A1})$$

and in the two-point correlation function between particles detected in  $V_1$  at time  $t_1$  and particles detected in  $V_2$  at time  $t_2$ , namely,

$$\mathbb{E}[n_1 n_2](t_1, t_2|x_0, t_0) = \sum_{n_1, n_2} n_1 n_2 \mathcal{P}(n_1, t_1, n_2, t_2|x_0, t_0). \quad (\text{A2})$$

By virtue of these considerations, it is therefore more convenient to introduce the probability-generating function associated to  $\mathcal{P}$ , namely,

$$W(z_1, z_2, x_0, t_0) = \sum_{n_1} \sum_{n_2} z_1^{n_1} z_2^{n_2} P(n_1, n_2, t_1, t_2|x_0, t_0), \quad (\text{A3})$$

where  $z_i$  is the conjugate variable of  $n_i$ ,  $i \in \{1, 2\}$ , and hence derive the equations for the (falling factorial) moments, which follow from

$$\mathbb{E}[n_1(n_1 - 1) \dots (n_1 - k + 1)n_2(n_2 - 1) \dots (n_2 - l + 1)](t_1, t_2|x_0, t_0) = \frac{\partial^{k+l}}{\partial z_1^k \partial z_2^l} W(z_1, z_2, x_0, t_0)|_{z_1=1, z_2=1}, \quad (\text{A4})$$

with  $k, l \geq 0$  and the normalization  $W(1, 1, x_0, t_0) = 1$ . It can be shown that  $W(z_1, z_2, x_0, t_0)$  satisfies the non-linear backward evolution equation

$$-\frac{\partial}{\partial t_0} W = \mathcal{D} \nabla_{x_0}^2 W - (\gamma + \beta)W + \beta G_p(W)G_d(W_d) + \gamma, \quad (\text{A5})$$

where  $G_p(z) = \sum_k z^k p_k$  is the probability-generating function associated to the prompt fission probability distribution  $p_k$  and  $G_d(z) = \sum_k z^k q_k$  is the probability-generating function for the precursor probability distribution  $q_k$ . The quantity  $W_d$  in Eq. (A5) is the probability-generating function associated to the creation of a precursor at  $(x_0, t_0)$ , namely,

$$W_d(z_1, z_2|x_0, t_0) = \lambda \int_{t_0}^{\infty} e^{-\lambda(t'-t_0)} W(z_1, z_2|x_0, t') dt'. \quad (\text{A6})$$

Taking the derivative of Eq. (A5) once with respect to  $z_1$  and using the definition in Eq. (A4), we obtain the evolution equation for the average neutron number in  $V_1$ , for a single starting particle in  $(x_0, t_0)$ :

$$\mathcal{L}^\dagger \mathbb{E}[n_1](t_1|x_0, t_0) = 0, \quad (\text{A7})$$

where  $\mathcal{L}^\dagger$  is the backward linear operator defined in Eq. (12). Equation (A7) (which coincides with Eq. (11) in the main text) is to be solved with the final condition

$$\mathbb{E}[n_1](t_1|x_0, t_0 = t_1) = \begin{cases} 1 & \text{if } x_0 \in V_1 \\ 0 & \text{otherwise.} \end{cases} \quad (\text{A8})$$

Letting  $\mathcal{G}(x, t, x_0, t_0)$  be the Green's function associated to the operator  $\mathcal{L}^\dagger$ , the solution to Eq. (A7) reads

$$\mathbb{E}[n_1](t_1|x_0, t_0) = \int dx' \chi_{V_1}(x') \mathcal{G}(x', t_1, x_0, t_0), \quad (\text{A9})$$

where  $\chi_V(x)$  is the characteristic function of a domain  $V$ .

Taking the mixed derivative of Eq. (A5) with respect to  $z_1$  and  $z_2$ , and using again the definition in Eq. (A4), we obtain the evolution equation for the two-point correlation function, for a single starting particle in  $(x_0, t_0)$ :

$$\mathcal{L}^\dagger \mathbb{E}[n_1 n_2](t_1, t_2|x_0, t_0) = -f_{\text{corr}}(t_1, t_2|x_0, t_0), \quad (\text{A10})$$

where we have defined

$$\begin{aligned} f_{\text{corr}}(t_1, t_2|x_0, t_0) &= \beta \nu_{p,2} \mathbb{E}[n_1] \mathbb{E}[n_2] + \beta \nu_{p,1} \nu_{d,1} \mathbb{E}[n_1] \lambda \int_{t_0}^{t_2} e^{-\lambda(t'-t_0)} \mathbb{E}[n_2](t') dt' \\ &+ \beta \nu_{p,1} \nu_{d,1} \mathbb{E}[n_2] \lambda \int_{t_0}^{t_1} e^{-\lambda(t'-t_0)} \mathbb{E}[n_1](t') dt' + \beta \nu_{d,2} \lambda^2 \int_{t_0}^{t_1} e^{-\lambda(t'-t_0)} \mathbb{E}[n_1](t') dt' \int_{t_0}^{t_2} e^{-\lambda(t'-t_0)} \mathbb{E}[n_2](t') dt' \end{aligned} \quad (\text{A11})$$

with the shorthand notation  $\mathbb{E}[n_i] = \mathbb{E}[n_i](t_1|x_0, t_0)$ ,  $i \in \{1, 2\}$ . Equation (A10) is to be solved with the final condition

$$\mathbb{E}[n_1 n_2](t_0 = t_1) = \begin{cases} \mathbb{E}[n_2](t_2|x_0, t_0 = t_1) & \text{if } x_0 \in V_1 \\ 0 & \text{otherwise.} \end{cases} \quad (\text{A12})$$

Using the Green's function associated to the operator  $\mathcal{L}^\dagger$ , the solution to Eq. (A10) can be expressed as

$$\mathbb{E}[n_1 n_2](t_1, t_2|x_0, t_0) = \int dx' \chi_{V_1}(x') \mathbb{E}[n_2](t_2|x', t_1) \mathcal{G}(x', t_1, x_0, t_0) + \int_{t_0}^{t_1} dt' \int dx' f_{\text{corr}}(t_1, t_2|x', t') \mathcal{G}(x', t', x_0, t_0). \quad (\text{A13})$$

Finally, the case of a collection of  $\mathcal{N}$  independent particles whose initial coordinates are distributed according to a given source  $\mathcal{Q}(x_0, t_0)$  can be dealt with by observing that the resulting probability-generating function  $W_{\mathcal{Q}}(z_1, z_2)$  is related to the one-particle probability-generating function  $W(z_1, z_2, x_0, t_0)$  by

$$W_{\mathcal{Q}_{\mathcal{N}}}(z_1, z_2) = \left[ \int_{-\infty}^{t_1} dt_0 \int dx_0 W(z_1, z_2, x_0, t_0) \mathcal{Q}(x_0, t_0) \right]^{\mathcal{N}}. \quad (\text{A14})$$

Then, by taking the derivative of Eq. (A14) once with respect to  $z_1$  we obtain the average number of particles in  $V_1$  for a collection of  $\mathcal{N}$  source particles:

$$\mathbb{E}[n_1](t_1|\mathcal{Q}_{\mathcal{N}}) = \mathcal{N} \int_{-\infty}^{t_1} dt_0 \int dx_0 \mathbb{E}[n_1](t_1|x_0, t_0) \mathcal{Q}(x_0, t_0). \quad (\text{A15})$$

Similarly, by taking the mixed derivative of Eq. (A14) with respect to  $z_1$  and  $z_2$  we obtain the pair correlation between detector  $V_1$  and  $V_2$  for a collection of  $\mathcal{N}$  source particles:

$$\begin{aligned} \mathbb{E}[n_1 n_2](t_1, t_2|\mathcal{Q}_{\mathcal{N}}) &= \mathcal{N}(\mathcal{N} - 1) \mathbb{E}[n_1](t_1|\mathcal{Q}_{\mathcal{N}}) \mathbb{E}[n_2](t_2|\mathcal{Q}_{\mathcal{N}}) \\ &+ \mathcal{N} \int_{-\infty}^{t_1} dt_0 \int dx_0 \mathbb{E}[n_1 n_2](t_1, t_2|x_0, t_0) \mathcal{Q}(x_0, t_0). \end{aligned} \quad (\text{A16})$$

The continuous version of Eqs. (A15) and (A16) can be obtained by centering the detector regions  $V_1$  and  $V_2$  around  $x_1$  and  $x_2$ , respectively, defining

$$\begin{aligned} n(x_1, t_1) &= \lim_{V_1 \rightarrow 0} \frac{\mathbb{E}[n_1](t_1|\mathcal{Q}_{\mathcal{N}})}{V_1} \\ u(x_1, t_1, x_2, t_2) &= \lim_{V_1, V_2 \rightarrow 0} \frac{\mathbb{E}[n_1 n_2](t_1, t_2|\mathcal{Q}_{\mathcal{N}})}{V_1 V_2} \end{aligned}$$

and letting the detector sizes shrink to zero, from which we recover Eqs. (20) and (21), respectively. Similarly, if we were to start our system with a collection of  $N$  neutrons, each having a source distribution  $\mathcal{Q}_n(x_0, t_0)$ , and  $M$  precursors, each having a source distribution  $\mathcal{Q}_m(x_0, t_0)$ , then Eq. (A14) would be replaced by

$$W_{\mathcal{Q}_{n+m}}(z_1, z_2) = \left[ \int_{-\infty}^{t_1} dt_0 \int dx_0 W(z_1, z_2, x_0, t_0) \mathcal{Q}_n(x_0, t_0) \right]^N \left[ \int_{-\infty}^{t_1} dt_0 \int dx_0 W(z_1, z_2, x_0, t_0) \mathcal{Q}_m(x_0, t_0) \right]^M. \quad (\text{A17})$$

Correspondingly, setting  $\mathcal{N} = N + M$  and denoting

$$\mathcal{Q}_{n+m}(x_0, t_0) = \frac{N}{N+M} \mathcal{Q}_n(x_0, t_0) + \frac{M}{N+M} \mathcal{Q}_m(x_0, t_0), \quad (\text{A18})$$

for the average number of particles we would have

$$\mathbb{E}[n_1](t_1|\mathcal{Q}_{n+m}) = \mathcal{N} \int_{-\infty}^{t_1} dt_0 \int dx_0 \mathbb{E}[n_1](t_1|x_0, t_0) \mathcal{Q}_{n+m}(x_0, t_0), \quad (\text{A19})$$

and for the pair correlation we would have

$$\begin{aligned} \mathbb{E}[n_1 n_2](t_1, t_2|\mathcal{Q}_{n+m}) &= \mathcal{N}^2 \mathbb{E}[n_1](t_1|\mathcal{Q}_{n+m}) \mathbb{E}[n_2](t_2|\mathcal{Q}_{n+m}) \\ &- N \mathbb{E}[n_1](t_1|\mathcal{Q}_n) \mathbb{E}[n_2](t_2|\mathcal{Q}_n) - M \mathbb{E}[n_1](t_1|\mathcal{Q}_m) \mathbb{E}[n_2](t_2|\mathcal{Q}_m) \\ &+ \mathcal{N} \int_{-\infty}^{t_1} dt_0 \int dx_0 \mathbb{E}[n_1 n_2](t_1, t_2|x_0, t_0) \mathcal{Q}_{n+m}(x_0, t_0). \end{aligned} \quad (\text{A20})$$

The Pál and Bell backward formalism can be easily extended to include more general detectors (for instance, an array  $\mathbf{V} = (V_1, \dots, V_K)$  of  $K$  non-overlapping regions), and to more general sources (for instance,  $N$  and  $M$  can be themselves random variables with Poisson distributions).

### Appendix B: Solutions for the anarchic model

For the critical anarchic model with a critical source, the solution of the pair correlation function in Eq. (A10) can be derived explicitly and is provided in this section for reference. For  $t_1 < t_2$ , the pair correlation function  $u(x_1, t_1, x_2, t_2)$  can be decomposed as follows:

$$u(x_1, t_1, x_2, t_2) = \frac{\mathcal{N}(\mathcal{N} - 1)\theta^2}{4L^2(1 + \theta)^2} + \frac{\mathcal{N}\theta}{2L(1 + \theta)}\mathcal{G}(x_2, t_2, x_1, t_1) \\ + \frac{\mathcal{N}\theta}{2L(1 + \theta)} [u_{pp}(x_1, t_1, x_2, t_2) + u_{pd}(x_1, t_1, x_2, t_2) + u_{dp}(x_1, t_1, x_2, t_2) + u_{dd}(x_1, t_1, x_2, t_2)]. \quad (\text{B1})$$

Each component is defined in terms of the respective eigenmode expansion, namely,

$$u_{pp} = \sum_k \varphi_k(x_1) \varphi_k^\dagger(x_2) u_{pp}^k \quad (\text{B2})$$

$$u_{pd} = \sum_k \varphi_k(x_1) \varphi_k^\dagger(x_2) u_{pd}^k \quad (\text{B3})$$

$$u_{dp} = \sum_k \varphi_k(x_1) \varphi_k^\dagger(x_2) u_{dp}^k \quad (\text{B4})$$

$$u_{dd} = \sum_k \varphi_k(x_1) \varphi_k^\dagger(x_2) u_{dd}^k. \quad (\text{B5})$$

For the prompt-prompt component  $u_{pp}^k$  we have:

$$u_{pp}^0(t_1, t_2) = \frac{\beta\nu_{p,2}}{(1 + \theta)^2} \left[ \theta^2 t_1 + \theta \left( \frac{e^{\omega_d t_1} - 1}{\omega_d} + \frac{e^{\omega_d t_2} - e^{\omega_d(t_2 - t_1)}}{\omega_d} \right) + \frac{e^{\omega_d(t_1 + t_2)} - e^{\omega_d(t_2 - t_1)}}{2\omega_d} \right], \quad (\text{B6})$$

where we have introduced  $\omega_d = -\tau_2^{-1} = -\beta\nu_{d,1} - \lambda$ , and

$$u_{pp}^k(t_1, t_2) = \frac{\beta\nu_{p,2}}{(\omega_k^+ - \omega_k^-)^2} \left[ \frac{(\omega_k^+ + \lambda)^2}{2\omega_k^+} \left( e^{\omega_k^+(t_1 + t_2)} - e^{\omega_k^+(t_2 - t_1)} \right) + \frac{(\omega_k^- + \lambda)^2}{2\omega_k^-} \left( e^{\omega_k^-(t_1 + t_2)} - e^{\omega_k^-(t_2 - t_1)} \right) \right. \\ \left. + \frac{(\omega_k^+ + \lambda)(\omega_k^- + \lambda)}{\omega_k^+ + \omega_k^-} \left( e^{\omega_k^+(t_2 - t_1)} + e^{\omega_k^-(t_2 - t_1)} - (e^{\omega_k^+ t_1 + \omega_k^- t_2} + e^{\omega_k^+ t_2 + \omega_k^- t_1}) \right) \right],$$

for  $k \geq 1$ . For the prompt-delayed component  $u_{pd}^k$  we have

$$u_{pd}^0(t_1, t_2) = \frac{\beta\nu_{d,1}\nu_{p,1}\theta}{(1 + \theta)^2} \left[ \theta t_1 + \frac{e^{\omega_d t_1} - 1}{\omega_d} + \frac{\theta(e^{\omega_d(t_2 - t_1)} - e^{\omega_d t_2})}{\omega_d} + \frac{e^{\omega_d(t_2 - t_1)} - e^{\omega_d(t_1 + t_2)}}{2\omega_d} \right] \quad (\text{B7})$$

and

$$u_{pd}^k(t_1, t_2) = \frac{\beta\lambda\nu_{d,1}\nu_{p,1}}{(\omega_k^+ - \omega_k^-)^2} \left[ (\omega_k^+ + \lambda) \left( \frac{e^{\omega_k^+(t_1 + t_2)} - e^{\omega_k^+(t_2 - t_1)}}{2\omega_k^+} + \frac{e^{\omega_k^-(t_2 - t_1)} - e^{\omega_k^+ t_1 + \omega_k^- t_2}}{\omega_k^+ + \omega_k^-} \right) \right. \\ \left. + (\omega_k^- + \lambda) \left( \frac{e^{\omega_k^+(t_2 - t_1)} - e^{\omega_k^+ t_2 + \omega_k^- t_1}}{\omega_k^+ + \omega_k^-} + \frac{e^{\omega_k^-(t_1 + t_2)} - e^{\omega_k^-(t_2 - t_1)}}{2\omega_k^-} \right) \right] \quad (\text{B8})$$

for  $k \geq 1$ . For the delayed-prompt component  $u_{dp}^k$  we have

$$u_{dp}^0(t_1, t_2) = \frac{\beta\nu_{d,1}\nu_{p,1}\theta}{(1 + \theta)^2} \left[ \theta t_1 + \theta \left( \frac{1 - e^{\omega_d t_1}}{\omega_d} \right) + \frac{e^{\omega_d t_2} - e^{\omega_d(t_2 - t_1)}}{\omega_d} + \frac{e^{\omega_d(t_1 - t_2)} - e^{\omega_d(t_2 + t_1)}}{2\omega_d} \right] \quad (\text{B9})$$

and

$$u_{dp}^k(t_1, t_2) = \frac{\beta\lambda\nu_{d,1}\nu_{p,1}}{(\omega_k^+ - \omega_k^-)^2} \left[ (\omega_k^+ + \lambda) \left( \frac{e^{\omega_k^+(t_1+t_2)} - e^{\omega_k^+(t_2-t_1)}}{2\omega_k^+} + \frac{e^{\omega_k^+(t_2-t_1)} - e^{\omega_k^+t_2 + \omega_k^-t_1}}{\omega_k^+ + \omega_k^-} \right) \right. \\ \left. + (\omega_k^- + \lambda) \left( \frac{e^{\omega_k^-(t_2-t_1)} - e^{\omega_k^+t_1 + \omega_k^-t_2}}{\omega_k^+ + \omega_k^-} + \frac{e^{\omega_k^-(t_1+t_2)} - e^{\omega_k^-(t_2-t_1)}}{2\omega_k^-} \right) \right] \quad (\text{B10})$$

for  $k \geq 1$ . Finally, for the delayed-delayed component  $u_{dd}^k$  we have

$$u_{dd}^0(t_1, t_2) = \frac{\beta\nu_{d,2}\theta^2}{(1+\theta)^2} \left[ t_1 + \frac{1 + e^{\omega_d(t_1-t_2)} - e^{\omega_d t_1} - e^{\omega_d t_2}}{\omega_d} + \frac{e^{\omega_d(t_1+t_2)} - e^{\omega_d(t_2-t_1)}}{2\omega_d} \right] \quad (\text{B11})$$

and

$$u_{dd}^k(t_1, t_2) = \frac{\beta\lambda^2\nu_{d,2}}{(\omega_k^+ - \omega_k^-)^2} \left[ \frac{e^{\omega_k^+(t_1+t_2)} - e^{\omega_k^+(t_2-t_1)}}{2\omega_k^+} + \frac{e^{\omega_k^-(t_1+t_2)} - e^{\omega_k^-(t_2-t_1)}}{2\omega_k^-} \right. \\ \left. + \frac{e^{\omega_k^+(t_2-t_1)} + e^{\omega_k^-(t_2-t_1)} - e^{\omega_k^+t_1 + \omega_k^-t_2} - e^{\omega_k^-t_1 + \omega_k^+t_2}}{\omega_k^+ + \omega_k^-} \right] \quad (\text{B12})$$

for  $k \geq 1$ . Note that Eq. (21) of the main text, which is applicable to generic values of  $t_1$  and  $t_2$ , is recovered by operating the substitutions  $t_1 \rightarrow \min\{t_1, t_2\}$  and  $t_2 \rightarrow \max\{t_1, t_2\}$  in Eq. (B1).

Taking  $t_1 = t_2 = t$ , we can obtain an expression for the mean-squared pair distance  $\langle r^2 \rangle(t)$ . For our case (reflection boundary conditions,  $\nu_{d,2} = 0$ ), the expression reads:

$$\langle r^2 \rangle(t) = \frac{\iint (x-y)^2 u(x, y, t) dx dy}{u(t, t)} \\ = \frac{2L^2}{3} \left( 1 - \frac{1}{N + u_0^{pp}(t) + u_0^{dp}(t) + u_{pd}^0(t)} \right) - \frac{64L^2}{N + u_{pp}^0(t) + u_{dp}^0(t) + u_{pd}^0(t)} \sum_{\substack{k=1 \\ k \text{ odd}}}^{+\infty} \frac{u_{pp}^k(t) + u_{dp}^k(t) + u_{pd}^k(t)}{(k\pi)^4} \quad (\text{B13})$$

### Appendix C: Forward formalism for the models with population control

When population control is enforced, particle histories are no longer independent and we have to resort to the forward formalism. Using the strategy proposed in [19], we partition the viable reactor space into a set of  $K$  equal segments of length  $\delta x = 2L/K$ , which we denote as  $V_k$ , with  $k \in \{1, \dots, K\}$ . Correspondingly, we write  $\mathbf{n} = (n_1, \dots, n_K)$ ,  $\mathbf{m} = (m_1, \dots, m_K)$ , and we denote by  $\mathcal{P}(\mathbf{n}, \mathbf{m}, t)$  the joint probability of observing  $n_k$  neutrons and  $m_k$  precursors in each of the  $K$  detectors at time  $t$ , for  $1 \leq k \leq K$ , given an initial condition with  $N$  neutrons and  $M$  precursors at time  $t_0 = 0$  uniformly distributed in space. The stochastic rules and the associated transition rates are those defined in Sec. IV. The evolution equations for  $\mathcal{P}(\mathbf{n}, \mathbf{m}, t)$  can be written more concisely introducing the annihilation  $a_k$  and creation  $a_k^\dagger$  operators, whose action on a state vector  $\mathbf{v} = (v_1, \dots, v_K)$  is defined by

$$a_k \mathbf{v} = (\dots, v_{k-1}, v_k - 1, v_{k+1}, \dots) \quad (\text{C1})$$

$$a_k^\dagger \mathbf{v} = (\dots, v_{k-1}, v_k + 1, v_{k+1}, \dots). \quad (\text{C2})$$

#### 1. Master equations

For the  $N$ -control model described in Sec. IV A, where exactly two neutrons and at most one precursor are produced in each fission event, and population control is enforced on neutrons alone, probability balance yields the master

equation

$$\begin{aligned}
\frac{\partial}{\partial t}\mathcal{P}(\mathbf{n}, \mathbf{m}, t) = & \sum_i \left[ \xi(n_{i+1} + 1)\mathcal{P}(a_{i+1}^\dagger a_i \mathbf{n}, \mathbf{m}, t) + \xi(n_{i-1} + 1)\mathcal{P}(a_{i-1}^\dagger a_i \mathbf{n}, \mathbf{m}, t) - 2\xi n_i \mathcal{P}(\mathbf{n}, \mathbf{m}, t) \right] \\
& + \beta(1 - \nu_{d,1})N \sum_{i,j \neq i} \left( \frac{n_i + 1}{N} \frac{n_j - 1}{N - 1} \mathcal{P}(a_i^\dagger a_j \mathbf{n}, \mathbf{m}, t) - \frac{n_i}{N} \frac{n_j}{N - 1} \mathcal{P}(\mathbf{n}, \mathbf{m}, t) \right) \\
& + \beta\nu_{d,1}N \sum_{i,j \neq i} \left( \frac{n_i + 1}{N} \frac{n_j - 1}{N - 1} \mathcal{P}(a_i^\dagger a_j \mathbf{n}, a_j \mathbf{m}, t) - \frac{n_i}{N} \frac{n_j}{N - 1} \mathcal{P}(\mathbf{n}, \mathbf{m}, t) \right) \\
& + \beta\nu_{d,1}N \sum_i \left( \frac{n_i}{N} \frac{n_i - 1}{N - 1} \mathcal{P}(\mathbf{n}, a_j \mathbf{m}, t) - \frac{n_i}{N} \frac{n_i - 1}{N - 1} \mathcal{P}(\mathbf{n}, \mathbf{m}, t) \right) \\
& + \lambda m \sum_{i,j \neq i} \left( \frac{m_i + 1}{m} \frac{n_j + 1}{N} \mathcal{P}(a_i a_j^\dagger \mathbf{n}, a_i^\dagger \mathbf{m}, t) - \frac{m_i}{m} \frac{n_j}{N} \mathcal{P}(\mathbf{n}, \mathbf{m}, t) \right) \\
& + \lambda m \sum_i \left( \frac{m_i + 1}{m} \frac{n_i}{N} \mathcal{P}(\mathbf{n}, a_i^\dagger \mathbf{m}, t) - \frac{m_i}{m} \frac{n_i}{N} \mathcal{P}(\mathbf{n}, \mathbf{m}, t) \right). \tag{C3}
\end{aligned}$$

where  $\xi$  is the diffusion rate of a neutron from one site to a neighbouring one,  $m = \sum_i m_i$  is the total number of precursors, and the total number of neutrons is  $n = \sum_i n_i = N$  because of population control. As a special case, when precursors are neglected ( $\lambda = 0$ ,  $\nu_{d,1} = 0$ ), Eq. (C3) degenerates into

$$\begin{aligned}
\frac{\partial}{\partial t}\mathcal{P}(\mathbf{n}, t) = & \sum_i \left[ \xi(n_{i+1} + 1)\mathcal{P}(a_{i+1}^\dagger a_i \mathbf{n}, t) + \xi(n_{i-1} + 1)\mathcal{P}(a_{i-1}^\dagger a_i \mathbf{n}, t) - 2\xi n_i \mathcal{P}(\mathbf{n}, t) \right. \\
& \left. + \sum_{j \neq i} \left( \beta N \frac{n_i + 1}{N} \frac{n_j - 1}{N - 1} \mathcal{P}(a_i^\dagger a_j \mathbf{n}, t) - \beta N \frac{n_i}{N} \frac{n_j}{N - 1} \mathcal{P}(\mathbf{n}, t) \right) \right],
\end{aligned}$$

which corresponds to the population control model proposed in Ref. 22 and revisited in Ref. 21. From Eq. (C3) the master equation for the total population sizes is easily derived, and, because of strict population control on  $N$ , it is an equation on  $m$  only, namely

$$\frac{\partial}{\partial t}\mathcal{P}(m, t) = \beta N \nu_{d,1} \mathcal{P}(m - 1, t) - \beta N \nu_{d,1} \mathcal{P}(m, t) + (m + 1)\lambda \mathcal{P}(m + 1, t) - m\lambda \mathcal{P}(m, t). \tag{C4}$$

By taking the moments of Eq. (C4), one derives Eqs. (29) and Eqs. (30) of the main text.

For the *NM-control* model described in Sec. IV B, where population control is enforced on neutrons and precursors,

probability balance yields the master equation

$$\begin{aligned}
\frac{\partial}{\partial t} \mathcal{P}(\mathbf{n}, \mathbf{m}, t) = & \sum_i \left[ \xi(n_{i+1} + 1) \mathcal{P}(a_{i+1}^\dagger a_i \mathbf{n}, \mathbf{m}, t) + \xi(n_{i-1} + 1) \mathcal{P}(a_{i-1}^\dagger a_i \mathbf{n}, \mathbf{m}, t) - 2\xi n_i \mathcal{P}(\mathbf{n}, \mathbf{m}, t) \right. \\
& \left. + \sum_{j \neq i} \left( \frac{\beta(1 - \nu_{d,1})}{N-1} (n_i + 1)(n_j - 1) \mathcal{P}(a_i^\dagger a_j \mathbf{n}, \mathbf{m}, t) - \frac{\beta(1 - \nu_{d,1})}{N-1} n_i n_j \mathcal{P}(\mathbf{n}, \mathbf{m}, t) \right) \right] \\
& + \frac{\beta \nu_{d,1}}{(N-1)M} \left[ \sum_{\substack{i,j,k \\ i \neq j \neq k}} \left( (n_i + 1)(n_j - 1)(m_k + 1) \mathcal{P}(a_i^\dagger a_j \mathbf{n}, a_j a_k^\dagger \mathbf{m}, t) - n_i n_j m_k \mathcal{P}(\mathbf{n}, \mathbf{m}, t) \right) \right. \\
& \sum_{\substack{i,k \\ i \neq k}} \left( n_i (n_i - 1)(m_k + 1) \mathcal{P}(\mathbf{n}, a_i a_k^\dagger \mathbf{m}, t) - n_i (n_i - 1) m_k \mathcal{P}(\mathbf{n}, \mathbf{m}, t) \right) \\
& \sum_{\substack{i,j \\ i \neq j}} \left( (n_i + 1)(n_j - 1)(m_i + 1) \mathcal{P}(a_i^\dagger a_j \mathbf{n}, a_i^\dagger a_j \mathbf{m}, t) - n_i n_j m_i \mathcal{P}(\mathbf{n}, \mathbf{m}, t) \right) \\
& \left. \sum_{\substack{i,j \\ i \neq j}} \left( (n_i + 1)(n_j - 1) m_j \mathcal{P}(a_i^\dagger a_j \mathbf{n}, \mathbf{m}, t) - n_i n_j m_j \mathcal{P}(\mathbf{n}, \mathbf{m}, t) \right) \right] \\
& + \frac{\lambda}{N} \sum_{\substack{i,j \\ i \neq j}} \left( m_i (n_j + 1) \mathcal{P}(a_i a_j^\dagger \mathbf{n}, \mathbf{m}, t) - m_i n_j \mathcal{P}(\mathbf{n}, \mathbf{m}, t) \right). \tag{C5}
\end{aligned}$$

with  $n = N$  and  $m = M$  at all times. Finally, for the *immigration model* described in Sec. IV C, probability balance yields the master equation

$$\begin{aligned}
\frac{\partial}{\partial t} \mathcal{P}(\mathbf{n}, t) = & \sum_i \left[ \xi(n_{i+1} + 1) \mathcal{P}(a_{i+1}^\dagger a_i \mathbf{n}, t) + \xi(n_{i-1} + 1) \mathcal{P}(a_{i-1}^\dagger a_i \mathbf{n}, t) - 2\xi n_i \mathcal{P}(\mathbf{n}, t) \right. \\
& \left. + \frac{\beta}{N-1} \sum_{j \neq i} \left( (n_i + 1)(n_j - 1) \mathcal{P}(a_i^\dagger a_j \mathbf{n}, t) - n_i n_j \mathcal{P}(\mathbf{n}, t) \right) + \frac{\lambda M}{N} \sum_{j \neq i} \mathcal{Q}_j \left( (n_i + 1) \mathcal{P}(a_i^\dagger a_j \mathbf{n}, t) - n_i \mathcal{P}(\mathbf{n}, t) \right) \right].
\end{aligned}$$

## 2. Moment equations

Once the master equations for the probability  $\mathcal{P}(\mathbf{n}, \mathbf{m}, t)$  have been established, the moments of the population are derived by summation: for the average densities we have

$$\mathbb{E}[n_i](t) = \sum_{\mathbf{n}, \mathbf{m}} n_i \mathcal{P}(\mathbf{n}, \mathbf{m}, t) \tag{C6a}$$

$$\mathbb{E}[m_i](t) = \sum_{\mathbf{n}, \mathbf{m}} m_i \mathcal{P}(\mathbf{n}, \mathbf{m}, t), \tag{C6b}$$

for  $i \in \{1, \dots, K\}$ . The two-point correlations between particles detected in  $V_i$  and particles detected in  $V_j$  at time  $t$  are similarly obtained from

$$\mathbb{E}[n_i n_j](t) = \sum_{\mathbf{n}, \mathbf{m}} n_i n_j \mathcal{P}(\mathbf{n}, \mathbf{m}, t) \tag{C7a}$$

$$\mathbb{E}[n_i m_j](t) = \sum_{\mathbf{n}, \mathbf{m}} n_i m_j \mathcal{P}(\mathbf{n}, \mathbf{m}, t) \tag{C7b}$$

$$\mathbb{E}[m_i m_j](t) = \sum_{\mathbf{n}, \mathbf{m}} m_i m_j \mathcal{P}(\mathbf{n}, \mathbf{m}, t), \tag{C7c}$$



for  $i, j \in \{1, \dots, K\}$ . For the  $N$ -control model, the discrete moment equations obtained directly from Eq. (C3) read

$$\frac{\partial}{\partial t} \mathbb{E}[n_i](t) = \xi \Delta \mathbb{E}[n_i](t) + \lambda \left( \mathbb{E}[m_i](t) - \frac{\mathbb{E}[n_i m](t)}{N} \right) \quad (\text{C8a})$$

$$\frac{\partial}{\partial t} \mathbb{E}[m_i](t) = \beta \nu_{d,1} \mathbb{E}[n_i](t) - \lambda \mathbb{E}[m_i](t) \quad (\text{C8b})$$

for the first spatial moment, and

$$\begin{aligned} \frac{\partial}{\partial t} \mathbb{E}[n_i n_j](t) &= \xi (\mathbb{E}[n_i \Delta n_j](t) + \mathbb{E}[n_j \Delta n_i](t)) - \frac{2\beta}{N_0 - 1} \mathbb{E}[n_i n_j](t) + \lambda C_N (\mathbb{E}[n_i m_j](t) + \mathbb{E}[m_i n_j](t)) \\ &\quad - \frac{2\lambda}{N} \mathbb{E}[n_i n_j m](t) + \frac{2\beta}{N_0 - 1} \delta_{i,j} N_0 \mathbb{E}[n_i](t) + \lambda \delta_{i,j} \left( \mathbb{E}[m_i](t) + \frac{\mathbb{E}[n_i m](t)}{N} \right) \\ &\quad + \delta_{i,j} \xi (\mathbb{E}[n_{i+1}](t) + \mathbb{E}[n_{i-1}](t) + 2\mathbb{E}[n_i](t)) - \delta_{i+1,j} \xi (\mathbb{E}[n_{i+1}](t) + \mathbb{E}[n_i](t)) \\ &\quad - \delta_{i-1,j} \xi (\mathbb{E}[n_i](t) + \mathbb{E}[n_{i-1}](t)) \end{aligned} \quad (\text{C9})$$

$$\begin{aligned} \frac{\partial}{\partial t} \mathbb{E}[n_i m_j](t) &= \xi \mathbb{E}[m_j \Delta n_i](t) - \lambda \frac{N-1}{N} \mathbb{E}[n_i m_j](t) - \lambda \frac{\mathbb{E}[n_i m_j m](t)}{N} \\ &\quad + \beta \nu_{d,1} C_{N-1} \mathbb{E}[n_i n_j](t) + \lambda \mathbb{E}[m_i m_j](t) + \delta_{i,j} \left( \frac{\beta \nu_{d,1} N}{N-1} \mathbb{E}[n_i](t) - \lambda \mathbb{E}[m_i](t) \right) \end{aligned} \quad (\text{C10})$$

$$\frac{\partial}{\partial t} \mathbb{E}[m_i m_j](t) = \beta \nu_{d,1} (\mathbb{E}[m_i n_j](t) + \mathbb{E}[n_i m_j](t)) - 2\lambda \mathbb{E}[m_i m_j](t) + \delta_{i,j} (\beta \nu_{d,1} \mathbb{E}[n_i](t) + \lambda \mathbb{E}[m_i](t)) \quad (\text{C11})$$

for the second spatial moment, where we define  $\Delta f_i = f_{i+1} - 2f_i + f_{i-1}$ .

For the  $NM$ -control model, we similarly obtain equations for the first spatial moments, namely

$$\frac{\partial}{\partial t} \mathbb{E}[n_i](t) = \xi \Delta \mathbb{E}[n_i](t) + \lambda \left( \mathbb{E}[m_i](t) - \mathbb{E}[n_i](t) \frac{M}{N} \right) \quad (\text{C12})$$

$$\frac{\partial}{\partial t} \mathbb{E}[m_i](t) = \beta \nu_{d,1} \left( \mathbb{E}[n_i](t) - \mathbb{E}[m_i](t) \frac{N}{M} \right). \quad (\text{C13})$$

The equations for the second spatial moment read

$$\begin{aligned} \frac{\partial}{\partial t} \mathbb{E}[n_i n_j](t) &= \xi (\mathbb{E}[n_i \Delta n_j](t) + \mathbb{E}[n_j \Delta n_i](t)) - \left( \frac{2\beta}{N-1} + \frac{2\lambda M}{N} \right) \mathbb{E}[n_i n_j](t) + \lambda C_N (\mathbb{E}[m_i n_j](t) + \mathbb{E}[n_i m_j](t)) \\ &\quad + \frac{2N\beta}{N-1} \delta_{i,j} \mathbb{E}[n_i](t) + \lambda \delta_{i,j} \left( \mathbb{E}[m_i](t) + \mathbb{E}[n_i](t) \frac{M}{N} \right) \\ &\quad + \delta_{i,j} \xi (\mathbb{E}[n_{i+1}](t) + \mathbb{E}[n_{i-1}](t) + 2\mathbb{E}[n_i](t)) - \delta_{i+1,j} \xi (\mathbb{E}[n_{i+1}](t) + \mathbb{E}[n_i](t)) \\ &\quad - \delta_{i-1,j} \xi (\mathbb{E}[n_i](t) + \mathbb{E}[n_{i-1}](t)) \end{aligned} \quad (\text{C14})$$

$$\begin{aligned} \frac{\partial}{\partial t} \mathbb{E}[n_i m_j](t) &= \xi \mathbb{E}[m_j \Delta n_i](t) - \left( \frac{\beta \nu_{d,1} N}{M} + \lambda \frac{M}{N} \right) \mathbb{E}[n_i m_j](t) + \beta \nu_{d,1} \frac{N-2}{N-1} \mathbb{E}[n_i n_j](t) + \lambda \mathbb{E}[m_i m_j](t) \\ &\quad + \frac{\beta \nu_{d,1} N}{(N-1)} \delta_{i,j} \mathbb{E}[n_i](t) \end{aligned} \quad (\text{C15})$$

$$\frac{\partial}{\partial t} \mathbb{E}[m_i m_j](t) = \beta \nu_{d,1} C_M (\mathbb{E}[m_i n_j](t) + \mathbb{E}[n_i m_j](t)) - \frac{2\beta \nu_{d,1} N}{M} \mathbb{E}[m_i m_j](t) + \beta \nu_{d,1} \delta_{i,j} \left( \mathbb{E}[n_i](t) + \mathbb{E}[m_i](t) \frac{N}{M} \right).$$

Finally, for the immigration model, the first spatial moment satisfies

$$\frac{\partial}{\partial t} \mathbb{E}[n_i](t) = \xi \Delta \mathbb{E}[n_i](t) - \frac{\lambda M}{N} \mathbb{E}[n_i](t) + \lambda M \mathcal{Q}_i, \quad (\text{C16})$$

where  $\mathcal{Q}_i$  is the intensity of the source in the  $i$ -th detector region. The equation for the second spatial moment reads

$$\begin{aligned} \frac{\partial}{\partial t} \mathbb{E}[n_i n_j](t) &= \xi (\mathbb{E}[n_i \Delta n_j](t) + \mathbb{E}[\Delta n_i n_j](t)) - \left( \frac{2\beta}{N-1} + \frac{2\lambda M}{N} \right) \mathbb{E}[n_i n_j](t) + \delta_{i,j} \frac{2N\beta}{N-1} \mathbb{E}[n_i](t) \\ &\quad + \lambda M \delta_{i,j} \left( \mathcal{Q}_i + \frac{\mathbb{E}[n_i](t)}{N} \right) + \lambda M \frac{N-1}{N} (\mathcal{Q}_j \mathbb{E}[n_i](t) + \mathcal{Q}_i \mathbb{E}[n_j](t)) \\ &\quad + \delta_{i,j} \xi (\mathbb{E}[n_{i+1}](t) + \mathbb{E}[n_{i-1}](t) + 2\mathbb{E}[n_i](t)) - \delta_{i+1,j} \xi (\mathbb{E}[n_{i+1}](t) + \mathbb{E}[n_i](t)) \\ &\quad - \delta_{i-1,j} \xi (\mathbb{E}[n_i](t) + \mathbb{E}[n_{i-1}](t)). \end{aligned} \quad (\text{C17})$$

Often, it is preferable to work with continuous observables: we therefore define the neutron and precursor densities by taking the limit

$$n(x, t|x_0, t_0) = \lim_{\delta x \rightarrow 0} \frac{\mathbb{E}[n_i](t|x_0, t_0)}{\delta x} \quad (\text{C18})$$

$$m(x, t|x_0, t_0) = \lim_{\delta x \rightarrow 0} \frac{\mathbb{E}[m_i](t|x_0, t_0)}{\delta x}, \quad (\text{C19})$$

Similarly, we define the pair correlation functions by taking the limits

$$u(x, y, t|x_0, t_0) = \lim_{\delta x \rightarrow 0} \frac{\mathbb{E}[n_i n_j](t|x_0, t_0)}{\delta x^2} \quad (\text{C20a})$$

$$v(x, y, t|x_0, t_0) = \lim_{\delta x \rightarrow 0} \frac{\mathbb{E}[n_i m_j](t|x_0, t_0)}{\delta x^2} \quad (\text{C20b})$$

$$w(x, y, t|x_0, t_0) = \lim_{\delta x \rightarrow 0} \frac{\mathbb{E}[m_i m_j](t|x_0, t_0)}{\delta x^2}, \quad (\text{C20c})$$

which describe the correlations at time  $t$  between a particle found at  $x$  and a particle found at  $y$ . The  $i$ -th ( $j$ -th) detector is defined to be the one containing  $x$  ( $y$ ). We also define the diffusion coefficient to be

$$\mathcal{D} = \lim_{\delta x \rightarrow 0} (\xi \delta x^2).$$

#### Appendix D: Solutions of the $NM$ -control model

We can obtain solutions to Eqs. (42) by using a Fourier decomposition which, for reflection boundary conditions, reduces to

$$f_\infty = \sum_{k=-\infty}^{+\infty} f_{k,k} \cos\left(\frac{k\pi}{2L}(L-x)\right) \cos\left(\frac{k\pi}{2L}(L-y)\right).$$

Indeed, in this case all the coefficients with  $k_1 \neq k_2$  are zero. The terms  $f_{k,k}$  thus read

$$\tilde{u}_{k,k} = \frac{m(N-1)\lambda^2 + n\beta \left( N(\alpha_1 + \tilde{k}^2 D) + 2(N-1)\nu_{d,1}\lambda \right)}{LN \left( \alpha_1 + \tilde{k}^2 D \right) \left( \tau_n + 2\tilde{k}^2 D \right) - 2L(N-2)\beta\nu_{d,1}\lambda} \quad (\text{D1})$$

$$v_{k,k} = \frac{2nN\beta \left( (N-1)\tau_n + (N-2)\beta + 2\tilde{k}^2(N-1)D \right) \nu_{d,1} + m(N-1)N \left( \tau_n + 2\tilde{k}^2 D \right) \lambda}{2L(N-1) \left( N(\alpha_1 + \tilde{k}^2 D)(\tau_n + 2\tilde{k}^2 D) - 2(N-2)\beta\nu_{d,1}\lambda \right)} \quad (\text{D2})$$

$$\tilde{w}_{k,k} = \frac{M-1}{N} \tilde{v}_{k,-k} \quad (\text{D3})$$

where  $\tau_n, \tau_c$  are given by Eqs. (43), and  $n, m$  and  $\tilde{k}$  are respectively given by

$$n = \frac{N}{2L}, \quad m = \frac{M}{2L}, \quad \tilde{k} = \frac{k\pi}{2L}.$$

---

\* theophile.bonnet@cea.fr

† davide.mancusi@cea.fr

‡ andrea.zoia@cea.fr

[1] T. E. Harris, *The Theory of Branching Processes* (Springer-Verlag (Berlin), 1963).

[2] H. C. Berg, *Random Walks in Biology* (Princeton University Press, 1993).

[3] M. M. R. Williams, *Random Processes in Nuclear Reactors*, 1st ed. (Pergamon Press, Oxford, New York, 1974).

[4] A. Bharucha-Reid, *Elements of the theory of Markov pro-*

- cesses and their applications (Mc Graw Hill, New-York, 1960).
- [5] M. Bartlett, *Stochastic Population Models in Ecology and Epidemiology*, Methuen's monographs on applied probability and statistics (Methuen, 1960).
- [6] I. Pázsit and L. Pál, *Neutron fluctuations: A Treatise on the Physics of Branching Processes* (Elsevier, 2007).
- [7] N. Bailey, *The Mathematical Theory of Infectious Diseases and Its Applications*, Mathematics in Medicine Series (Griffin, 1975).
- [8] D. G. Kendall, Deterministic and stochastic epidemics in closed populations, in *Volume 4 Contributions to Biology and Problems of Health*, edited by J. Neymann (University of California Press, 2020) pp. 149–166.
- [9] G. Bell and S. Glasstone, *Nuclear Reactor Theory* (Van Nostrand Reinhold Company, 1970).
- [10] M. Aguiar, J. Van-Dierdonck, J. Mar, *et al.*, *Sci. Rep.* **11**, 13839 (2021).
- [11] E. Dumonteil, S. N. Majumdar, A. Rosso, and A. Zoia, *Proceedings of the National Academy of Sciences* **110**, 4239 (2013).
- [12] D. Balcan, B. Gonçalves, H. Hu, J. Ramasco, V. Colizza, and A. Vespignani, *J. Comput. Sci.* **1**, 132 (2010).
- [13] D. Balcan, V. Colizza, B. Gonçalves, H. Hu, J. J. Ramasco, and A. Vespignani, *Proceedings of the National Academy of Sciences* **106**, 21484 (2009).
- [14] E. Dumonteil, R. Bahran, T. Cutler, *et al.*, *Commun. Phys.* **4**, 151 (2021).
- [15] J. M. Verbeke and O. Petit, *Nuclear Science and Engineering* **183** (2016).
- [16] S. Kim and M. C. Castro, *International Journal of Infectious Diseases* **98**, 328 (2020).
- [17] V. Colizza and A. Vespignani, *Journal of Theoretical Biology* **251**, 450 (2008).
- [18] A. Zoia, E. Dumonteil, A. Mazzolo, C. de Mulatier, and A. Rosso, *Physical Review E* **90**, 042118 (2014).
- [19] B. Houchmandzadeh, E. Dumonteil, A. Mazzolo, and A. Zoia, *Physical Review E* **92**, 052114 (2015).
- [20] A. Zoia and E. Dumonteil, in *M&C 2017, International Conference on Mathematics and Computational Methods Applied to Nuclear Science and Engineering* (Jeju, South Korea, 2017).
- [21] C. de Mulatier, E. Dumonteil, A. Rosso, and A. Zoia, *Journal of Statistical Mechanics: Theory and Experiment*, P08021 (2015).
- [22] M. Meyer, S. Havlin, and A. Bunde, *Physical Review E* **54**, 5567 (1996).
- [23] E. Dumonteil, F. Malvagi, A. Zoia, A. Mazzolo, D. Artusio, C. Dieudonné, and C. De Mulatier, *Annals of Nuclear Energy* **63**, 612 (2014).
- [24] Y. C. Zhang, M. Serva, and M. Polikarpov, *Journal of Statistical Physics* **58**, 849 (1990).
- [25] L. Pál and I. Pázsit, *Physica Scripta* **74**, 62 (2006).
- [26] T. M. Sutton and A. Mittal, *Nuclear Engineering and Technology* **49**, 1211 (2017), special Issue on International Conference on Mathematics and Computational Methods Applied to Nuclear Science and Engineering 2017 (M&C 2017).